ADVANCED FUNCTIONAL MATERIALS
www.afm-journal.de

State-of-the-Art Progress in Diverse Heterostructured Photocatalysts toward Promoting Photocatalytic Performance

Haijin Li, Yong Zhou, Wenguang Tu, Jinhua Ye, and Zhigang Zou**

Semiconductor photocatalysts have received much attention in recent years due to their great potentials for the development of renewable energy technologies, as well as for environmental protection and remediation. The effective harvesting of solar energy and suppression of charge carrier recombination are two key aspects in photocatalysis. The formation of heterostructured photocatalysts is a promising strategy to improve photocatalytic activity, which is superior to that of their single component photocatalysts. This Feature Article concisely summarizes and highlights the state-of-the-art progress of semiconductor/semiconductor heterostructured photocatalysts with diverse models, including type-I and type-II heterojunctions, Z-scheme system, p–n heterojunctions, and homojunction band alignments, which were explored for effective improvement of photocatalytic activity through increase of the visible-light absorption, promotion of separation, and transportation of the photoinduced charge carries, and enhancement of the photocatalytic stability.

1. Introduction

Utilization of renewable and clean energy resources and development of eco-friendly practical systems for environmental remediation have been drawing increasing attention, because environmental problems and energy consumption have been becoming the overwhelming problems for human in the new century. Therefore, the exploration of highly active photocatalyst systems for directly harvesting and converting solar energy into usable energy format is one of the promising strategies, owing to its utilization of non-polluting and abundant sunlight as a source of energy. The semiconductor photocatalysts are widely used to split water into H_2 and O_2,[1,2] photoreduce CO_2 into renewable fuels, such as CH_3OH, CH_4, and CO,[3–5] and decompose various organic contaminations to remedy our environment.[6,7] Many studies have been devoted to develop new and efficient photocatalysts and explore the fundamental factors that govern the photocatalytic activity.

The photocatalytic reaction primarily involves three main processes: i) the generation of electron-hole pairs after the absorption of light by photocatalysts; ii) the charge separation and migration onto the surface of photocatalysts; iii) the reduction/oxidation reaction on the surface of photocatalysts.[8–10] In depth, an efficient photocatalyst requires the semiconductor with suitable band gap for harvesting light, facile separation and transportation of charge carriers, and proper valence band

Dr. H. J. Li, Prof. Y. Zhou, W. G. Tu
Key Laboratory of Modern Acoustics (MOE)
Institute of Acoustics
Department of Physics
Nanjing University
Nanjing 210093, Jiangsu, P. R. China
E-mail: zhouyong1999@nju.edu.cn
Dr. H. J. Li
School of Mathematics and Physics
Institute of Optoelectronic Information Materials and Technology
Anhui University of Technology
Ma'anshan 243002, Anhui, P. R. China
Dr. H. J. Li, Prof. Y. Zhou, W. G. Tu, Prof. Z. G. Zou
Jiangsu Key Laboratory for Nano Technology
Eco-Materials and Renewable Energy Research Center (ERERC)
National Laboratory of Solid State Microstructures
and Department of Physics
Nanjing University
Nanjing 210093, Jiangsu, P. R. China
E-mail: zgzou@nju.edu.cn
Prof. Y. Zhou
Collaborative Innovation Center
of Advanced Microstructures
Nanjing University
Nanjing 210093, Jiangsu, P. R. China
Prof. J. Ye
Environmental Remediation Materials Unit
National Institute for Materials Science (NIMS)
1-1 Namiki, Tsukuba, Ibaraki 305–0044, Japan
Prof. J. Ye
TU-NIMS Joint Reseach Center
School of Material Science and Engineering
Tianjin University
92 Weijin Road, Tianjin, P. R. China

DOI: 10.1002/adfm.201401636

Haijin Li received his BS in Material Science and Technology from Zhengzhou University, China (2003). In 2008, he received his PhD from Institute of Solid State Physics (ISSP), Chinese Academy of Sciences (CAS). He joined the faculty at Anhui University of Technology in 2008. He is currently a Post-doctoral research fellow in ERERC, School of Physics, National Laboratory of Solid State Microstructures, Nanjing University, China. His main research is focused on the design and synthesis of heterostructure photocatalysis and their application.

Yong Zhou studied chemistry and physics at the University of Science and Technology of China (USTC), received his Ph.D. degree there in 2000. After working in Kyoto University in 2000–01, Max Planck Institute of Colloids and Interfaces in 2002–03, the National Institute of Materials Science (NIMS, Japan) in 2003–04, National Institute of Advanced Industrial Science and Technology (AIST, Japan) in 2004–08, and National University of Singapore (NUS) in 2008–09, he joined as a full professor in the Eco-materials and Renewable Energy Research Center (ERERC), School of Physics, National Laboratory of Solid State Microstructures, Nanjing University, China. His research now focuses on design and fabrication of solar-light driven clean energy materials for photocatalysis and flexible solar cells.

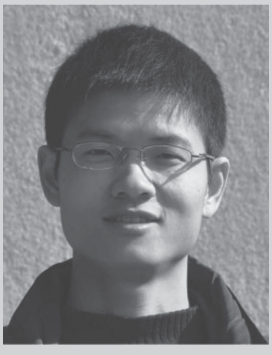

Wenguang Tu obtained his BS degree in 2010 from Southwest University, China. He is pursuing his PhD degree under the guidance of Prof. Yong Zhou in ERERC, School of Physics, National Laboratory of Solid State Microstructures, Nanjing University, China. His current research involves the synthesis of graphene-based nanomaterials for photocatalysis application.

Jinhua Ye received her PhD from the University of Tokyo in 1990. After that, she joined Osaka University as a faculty staff, and then moved to National Research Institute for Metals (former name of NIMS) 18 months later. She was appointed as the managing director of Photocatalytic Materials Center in 2006. She is currently the director of Research Unit for Environmental Remediation Materials, and a Principle Investigator of International Center for Materials Nanoarchitectonics (MANA), NIMS. She is also an adjunct Professor in Department of Chemistry, Hokkaido University. Her current research interests focus on photofunctional materials and their applications in the fields of environment remediation and new energy production.

Zhigang Zou received his bachelor degree and master degree from Tianjing University (China) in 1982 and 1986, respectively. He was a lecturer of Tianjing University from September 1986 to March 1991. Then, he moved to the Research Laboratory of Engineering Materials at the Tokyo Institute of Technology (Japan) as a visiting Researcher. After he received his PhD degree from the University of Tokyo (Japan) in 1996, he was a researcher at the Photoreaction Control Research Center, National Institute of Advanced Industrial Science and Technology (AIST), Japan. He has been with the Department of Physics at Nanjing University (China) as a distinguished professor of the Chang Jiang Scholars Program since 2003. He is also a Director of the Ecomaterials and Renewable Energy Research Center, Nanjing University. His current research interests are photocatalysis, solar cells, and fuel cells.

(VB) and conduction band (CB) edge potential for redox reaction being thermodynamically feasible. To date, much effort has been made to enhance the photocatalytic efficiencies of photocatalysts, such as doping and surface modification. Although some single semiconductor photocatalysts demonstrate high photocatalytic efficiency,[11–14] it is difficult to satisfy above these harsh terms simultaneously on a single semiconductor photocatalyst. The construction of heterostructured photocatalyst systems comprising multicomponent or multiphase is one of most effective strategies to balance the harsh terms, owing to the

tunable band structures and efficient electron-hole separation and transportation, which endow them with suitable properties superior to those of their individual components.

One popular strategy is the modification of single photocatalyst materials with metal nanoparticles, forming metal/semiconductor heterostructured photocatalysts. The surface plasmon resonance (SPR) effects and Schottky junction are very important to improvement of photocatalytic efficiency of metal/semiconductor heterostructured photocatalysts.[15–18] For example, under ultraviolet (UV) light irradiation, a built-in electric field near the interface of Au/TiO_2 appeared due to the existence of the Schottky junction. The photo-induced electrons in TiO_2 may flow into Au particles leaving holes in the valence band of TiO_2, and hence significantly separated the charge carriers; on the other hand, under visible light irradiation, the photoproduced electrons in Au particles transferred to TiO_2 due to the SPR effect of Au particles, which greatly improved solar energy conversion because of enhanced light absorption and scattering at the interface of Au/TiO_2.[15,16,18] Another important strategy to reduce charge carrier recombination probability is the formation of carbon group materials/semiconductor heterostructured photocatalysts.[5,19–21] Robust hollow spheres consisting of molecular-scale $Ti_{0.91}O_2$ nanosheets and graphene nanosheets as building blocks were fabricated, and presented high efficiency for photocatalytic CO_2 conversion into renewable fuel.[21] While comprehensive coverage of metal/semiconductor and carbon group materials/semiconductor heterostructured photocatalysts have been surveyed elsewhere,[19,22–26] the present Feature Article aims to concisely summarize and highlight the state-of-the-art progress of semiconductor/semiconductor heterostructured photocatalysts with diverse models, including type-I and type-II herterojunctions, Z-scheme, p–n heterojunctions, and homojunction band alignments. Based on these heterostructures, effective improvement of photocatalytic activity of photocatalysts was explored through increase of the visible-light absorption, promotion of separation and transportation of the charge carries, and enhancement of the photocatalytic stability. We do not attentionally categorize the heterostructured photocatalysts based on the reaction systems, for examples, photocatalytic and photoelectrochemical reactions as both systems face common challenges for high efficiency, which can be gained through similar strategies although the powder photocatalytic systems and photoelectrochemical cell systems may not share totally same working principles in the photocatalytic reaction.

2. Techniques for Synthesis of Heterostructured Photocatalysts

Various synthesis techniques, such as chemical vapor deposition (CVD), atomic layer deposition (ALD), hot-injection, hydrothermal/solvothermal method, successive ionic layer adsorption and reaction (SILAR), and ion exchange reaction, were developed to fabricate high-quality heterostructured photocatalysts.

2.1. CVD and ALD Routes

The CVD route is commonly used for heterojunction preparation, which allows for multiple materials to be deposited on suitable substrates in sequence. Heterostructured photocatalysts are generally prepared by two-step growth procedure. Firstly, the inner core semiconductor is grown on a suitable substrate via CVD or other synthetic methods. Secondly, the outer-layer shell semiconductor is subsequently deposited on the core surface under the optimized CVD conditions (such as deposition temperature, pressure, carrier gas, and evaporation time). Recently, our group fabricated high-quality WO_3/CdS core/shell nanowire arrays via a two-step CVD method.[27] Single crystalline WO_3 nanowire arrays were obtained on the tungsten foil substrate, followed by the CVD deposition of a homogenous shell of CdS nanoparticles. The similar ZnO/CdSSe core/shell arrays with controlled composition and shell thickness were also synthesized through the CVD deposition of CdSSe on the pre-grown ZnO nanowire arrays.[28] The formation of Zn containing alloy in the interface of core/shell heterojunction facilitated the growth of single-crystalline CdSSe shell layers through reducing both the lattice mismatch and the number of defect sites at the interface. Furthermore, other one-dimensional (1D) heterostructured photocatalyst systems, such as SnO_2/TiO_2,[29] and $SnO_2/(Ti_{0.5}V_{0.5})_2O_3$,[30] have also been synthesized by the CVD route.

Although sharing similar chemistry with CVD, ALD has attracted more attention in the area of heterostructured photocatalysts due to precisely controlling film thickness at the atomic level and conformal growth of complex nanostructures.[31–34] The photocatalytic active of heterostructured photocatalysts prepared by ALD is observably enhanced due to the improvement of light trapping and carrier separation.[31,32] The excellent conformability offered by ALD makes it possible to form homojunctions in a semiconductor through doping control with low defect densities. Through growth control, Wang and co-workers successfully produced n-p homejunctions within Fe_2O_3 by ALD.[31] More importantly, no obvious structural defects between p- and n-type Fe_2O_3 were observed, and a nominal 200 mV turn-on voltage shift toward the cathodic direction was measured, suggesting that the desired energetics for solar water splitting could achieve through advanced material preparations.

2.2. Hot-Injection and SILAR Approaches

The hot-injection method is often used to prepare the core/shell heterostructured nanocrystals (NCs). The method generally consists of two-step procedure. The first one involves initial synthesis of core material, followed by a purification step (in order to eliminate byproducts, unreacted precursors, and solvents); the second one involves the subsequent growth of the shell. In order to prevent nucleation of the shell material and uncontrolled ripening of the core material, the temperature for the shell growth is typically lower than that for the core synthesis. With this technique, the molecular precursors are rapidly decomposed at elevated temperature to produce a burst of NC nuclei followed by uniform steady state growth.[35–37] Moreover, a "one-pot" hot-injection approach without purification was also developed, which can be realized only if both the core and shell semiconductors are grown controllably in the same reaction mixture.[37] For ZnSe/CdS nanobarbells fabricated with

the one-opt method,[38] the CdS nanorods were synthesized using a seeded-type method by introducing small-diameter CdS NCs into the reaction mixture for the nucleus growth of linear CdS extensions, followed by injecting the precursors of Zn and Se solutions to grow ZnSe tips on CdS nanorods. A one-step synthetic method was also utilized for preparation of CdSe/ZnS core/shell NCs.[39] Due to the reactivity difference between Cd and Zn precursors with Se and S precursors, Cd- and Se (with a bit of S)-based cores and Zn- and S-based shells were generated successively, leading to the formation of the core/shell nanostructure with composition gradients, which relieved the lattice mismatch between cores and shells. This relatively simple "one-pot" method was also used to successfully fabricate CdSe/ZnSe NCs.[40]

The SILAR technique was also originally developed from solution baths. This method can effectively suppress homogenous nucleation, attributed to the decrease in the coexistence of cations and anions for the shell materials in solution. The precise control of shell thickness could be achieved by alternating injections of cationic and anionic precursors. For synthesis of CdS/ZnS core/shell NCs with the SILAR method,[41–43] CdS NCs with tunable particle size were firstly synthesized via a hot-injection approach. Zn and S precursors were then alternatively injected into the mixture solution of CdS and oleylamine for growth of ZnS shells with different thickness. Other heterostructures can also be easily obtained by the similar SILAR technique, such as CdSe/ZnS quantum dots (QDs)[44] and CdSe/CdS QDs.[45]

2.3. Hydrothermal/Solvothermal Methods

Hydrothermal/solvothermal methods are conveniently used for preparation of nanostructured photocatalysts. This method not only accelerates the dissolution of precursors but also speeds up the reaction rate between the precursors and the reagents, assigned to special reaction environment simultaneously with both the relatively high pressure and high temperature. For the In_2O_3/In_2S_3 core/shell nanorods, as-prepared In_2O_3 nanorod core was hydrothermally treated with S precursor solution to gradually convert In_2O_3 on the nanorod surfaces into In_2S_3 shells with controllable thickness determined by the reaction temperature.[46] Bi_2S_3/CdS heterostructures composed of Bi_2S_3 nanowires with triangle-like CdS NCs at their surfaces were constructed via one-pot reaction or two-step hydrothermal reaction.[47] CdS/TiO_2 core/shell nanocomposites were synthesized via a two-step solvothermal method.[48] The CdS nanowire core with the length of 2–3 μm and the diameter of 50–100 nm were initially synthesized with a solvothermal route. Then, a certain amount of as-preared CdS nanowires and tetrabutyl titanate were sonicated thoroughly in the mixture solution of absolute ethanol and deionized water, followed by solvothermal treatment. TiO_2 particles were thus densely coated onto the wall of the CdS nanowires to form the CdS/TiO_2 core/shell heterostructure.

2.4. Ion Exchange Reaction

Ion exchange is a novel approach to synthesize heterostructured photocatalysts through exchanging the ions at the interface of two semiconductors.[49–51] The shell is initially formed in gas or solution phase. In the process of cation exchange, external cations enter the parent crystal, and the original cations simultaneously diffuse out of the crystal. The ion exchange reaction is superior in terms of the selective formation of a dimer structure with an epitaxial heterointerface without changing the prototypical shape of the ionic semiconductor. ZnO/In_2S_3 core/shell nanorods were successfully synthesized via an ion-exchange reaction between ($Zn^{2+}O^{2-}$) ions and ($In^{3+}S^{2-}$) ions through the surface of the ZnO core, leading to the formation of an In_2S_3 layer over the ZnO nanorods.[52]

In addition, several other strategies have also been explored to synthesize heterostructured photocatalysts, such as electrochemical deposition,[35–38] chemical deposition,[39–41] and sol-gel method.[53–55] ZnO/CdS core/shell nanorod arrays were prepared directly on FTO (fluorine doped tin oxide) substrates via a two-step electrochemical deposition process.[56] ZnO nanorods were initially synthesized on FTO substrates via galvanostatic electrolysis in aqueous solution of Zn^{2+}, NH_4Ac (CH_3COONH_4), and $C_6H_{12}N_4$. The length and diameter of the ZnO nanorod can be controlled by changing the electrodeposition time. The CdS shell with tunable thickness on the ZnO nanorod surface was obtained in mixture solutions of Cd^{2+}, thiourea, DMSO (dimethyl sulfoxide), and H_2O.

3. Diverse Heterostructure Photocatalysts

To design a heterostructure system with highly photocatalytic activity, the key challenge is to optimize bandgap of each semiconductor component for harvesting solar light, especially the visible light, and prevent the recombination of photogenerated electron-hole pairs.[57] The heterojunctions provide an offset in the energies of the CB and/or VB edges to facilely enable the effective separation of photoexcited electron-hole pairs and subsequent transfer across the interface in the junction region, leading to enhanced photocatalytic performance. Heterostructured photocatalysts are widely applied in the following fields: 1) water splitting, 2) photodegradation of organic contaminants, and 3) photocatalytic conversion of CO_2 to renewable fuels. **Table 1** lists recent prominent heterostructured photocatalysts as well as their photocatalytic application.

According to the bandgap and electronic energy level of the semiconductors, the semiconductor heterojunctions can be primarily divided into five different cases: straddling alignment (type-I), staggered alignment (type-II), Z-scheme system, p–n heterojunctions, and homojunctions. The band gap, the electron affinity (lowest potential of CB), and the work function (highest potential of VB) of the combined semiconductors determine the dynamics of the electron and hole in the semiconductor heterojunctions.[58,59]

3.1. Type-I Heterostructures

In type-I band alignment, both VB and CB edges of semiconductor 2 are localized within the energy gap of semiconductor 1, forming straddling band alignment (**Figure 1**a). The VB and CB potentials of two different semiconductors play a crucial

Table 1. Recent report of diverse heterostructured photocatalysts for water splitting, degradation or oxidization of organic contaminants, and CO_2 conversion

	Water splitting	Degradation or oxidization of organic contaminants	CO_2 conversion
Type-I	CdSe/CdS,[64] CdS/ZnS,[41] In_2O_3/In_2S_3[46]	Bi_2S_3/CdS,[62] $V_2O_5/BiVO_4$[60]	Bi_2S_3/CdS[61]
Type-II	CdS/TiO_2,[70,99,110] CdSe/ TiO_2,[114] $SrTiO_3/TiO_2$,[97,98] Fe_2O_3/TiO_2,[77] ZnO/CdS,[118] In_2O_3/Ta_2O_5,[80] Fe_4N/Fe_2O_3,[93] $AgIn_5S_8/TiO_2$,[84] TiO_2/CdS/CdSe,[125] ZnO/CdS/CdSe,[131] CdS-CdSSe-CdSe/TiO_2,[133] ZnO/CdSSe[134]	CdS/TiO_2,[48,67,68,71,72] Bi_2S_3/TiO_2,[67] WO_3/TiO_2,[73–75] Fe_2O_3/TiO_2,[76] In_2O_3/TiO_2,[100,101] $ZnFe_2O_4/TiO_2$,[116] Fe_2O_3/WO_3,[81] ZnO/CdTe,[121] ZnO/In_2S_3,[52] ZnO/CdS,[117] $SrTiO_3/TiO_2$,[95] $BiVO_4/CeO_2$,[83] α-Fe_2O_3/CdS,[102] CdS/$ZnFe_2O_4$,[86] CdS/$CoFe_2O_4$,[86] Ag_3VO_4/TiO_2[85]	AgBr/TiO_2,[78] CeO2/TiO_2[79]
p–n	$CuFe_2O_4/TiO_2$,[141] CuO/ZnO,[145] $CaFe_2O_4$/TaON,[154] MoS_2/CdS[149,205]	Ag_2O/TiO_2,[138] $CuInSe_2/TiO_2$,[140] TiO_2/ZnO,[155] $ZnFe_2O_4$/TiO_2,[139] NiO/ZnO,[142] CuO/ZnO,[146] Cu_2O/ZnO,[147,148] $CuInS_2$/ZnO,[143] $CuInSe_2$/ZnO,[143] CuO/In_2O_3,[150] Ag_3PO_4/$BiVO_4$,[153] $Co_3O_4/BiVO_4$[152]	
Homojunction	anatase/rutile TiO_2,[158] α/β-Ga_2O_3,[165] p–n Cu_2O,[169] p–n Mg-doped Fe_2O_3/Fe_2O_3,[168] W-doped $BiVO_4$,[173] twin-induced $Cd_{0.5}Zn_{0.5}S$[175,176]	N-doped anatase/brookite TiO_2,[157] anatase/rutile TiO_2,[159,163] α/γ-Bi_2O_3,[164] the QDs/nanosheets Bi_2WO_6,[167] p–n Cu_2O,[170] p–n Co-doped TiO_2/TiO_2,[161] p–n Fe-doped TiO_2/TiO_2,[160] p–n Co-doped zincblende/wurtzite ZnO,[166] Pt/n-Si/n^+-Si/Ag[174]	
Z-scheme	CdS/Au/$TiO_{1.96}C_{0.04}$,[194] WO_3/W/$PbBi_2Nb_{1.9}Ti_{0.1}O_9$,[197] ZnO/CdS,[202] CdS/Au/ZnO[200]	$CaFe_2O_4/WO_3$,[204] CdS/Au/TiO_2[196]	CuO/TiO_2[203]

role in determination of the physical features of photogenerated charges and the photocatalytic performance. Typically for V_2O_5/$BiVO_4$ heterostructured photocatalysts,[60] the CB potential level of $BiVO_4$ is more negative than that of V_2O_5 so that photogenerated electrons could migrate from $BiVO_4$ to V_2O_5 driven by the contact electric field. As the VB potentials of $BiVO_4$ (2.77 eV) and V_2O_5 (2.73 eV) are very close, the photoexcited holes is hard to transfer from the VB of $BiVO_4$ to the VB of V_2O_5. Therefore, $V_2O_5/BiVO_4$ photocatalysts showed great increase in the separation extent and lifetime of the photogenerated electrons, leading to effective photodegradation of methylene blue (MB) under visible light irradiation. Type-I Bi_2S_3/CdS heterostructured photocatalyst shows photocatalytic reduction of CO_2 with H_2O into methanol with the yield of 613 μmol g^{-1} under visible light

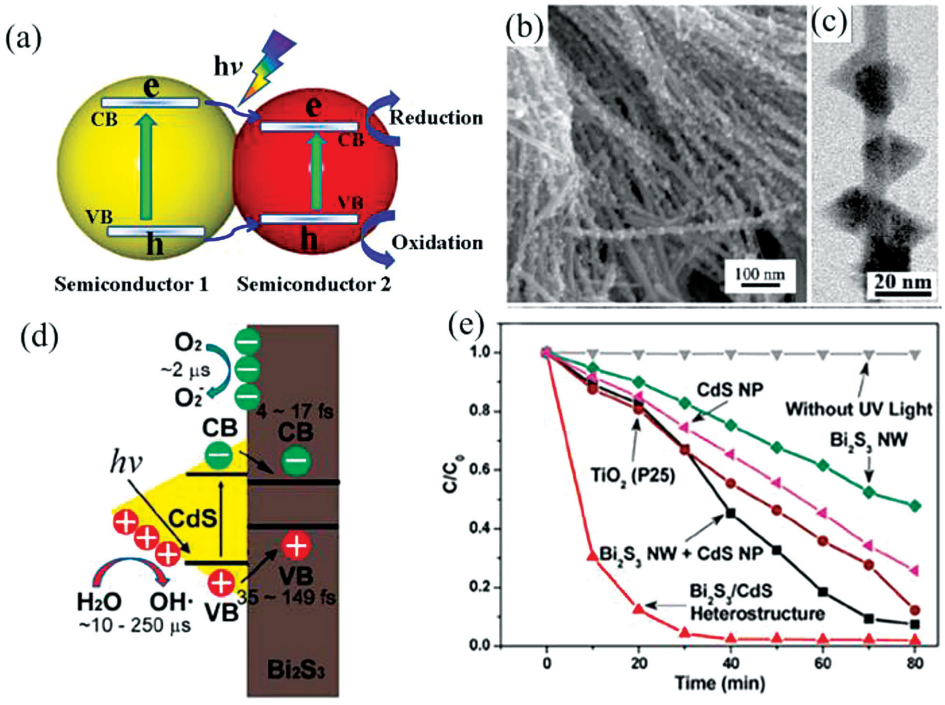

Figure 1. a) Schematic illustration of the type-I band alignments and the correspondingly possible separation and transfer process of photoinduced electron-hole pairs of semiconductor heterostructured photocatalysts. b) SEM and c) TEM images of Bi_2S_3/CdS heterostructures. d) Schematic diagram of electron-hole pair separation in Bi_2S_3/CdS heterostructures. e) Summary of photodegradation rate of methyl red (MR) with various catalysts under ultraviolet (UV) light. Reproduced with permission.[60] Copyright 2011, American Chemical Society.

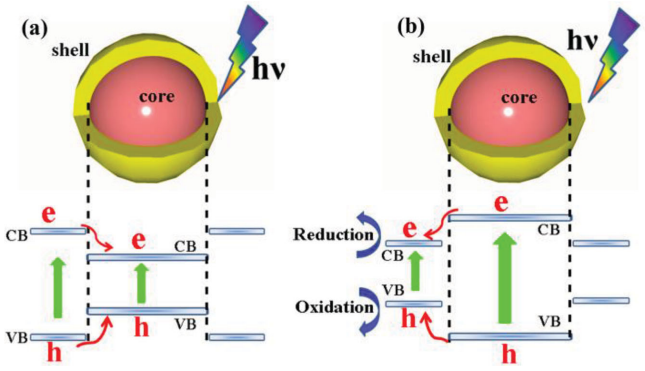

Figure 2. Schematic illustrations of the a) type-I and b) inverted type-I core/shell heterostructures band alignments, and the correspondingly possible separation and transfer process of photoinduced electron-hole pairs of semiconductor photocatalysts.

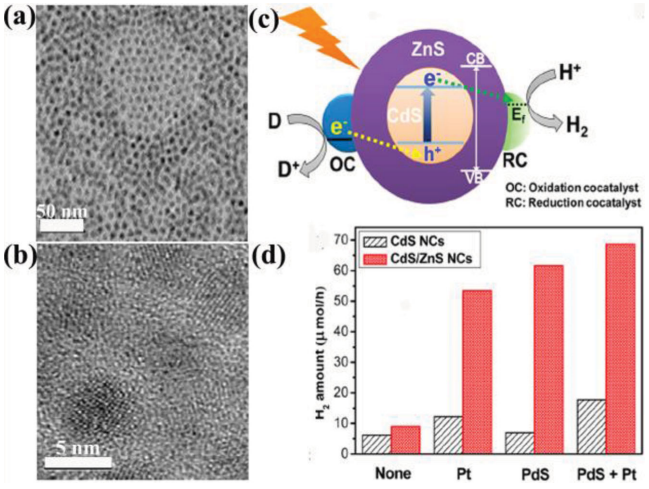

Figure 3. TEM images of a) CdS/ZnS NCs dispersed in Chloroform. b) HRTEM image of the CdS/ZnS NCs. c) Schematic description of the transfer and separation of the photogenerated electrons and holes from type-I Core/Shell NCs. d) Photocatalytic activities of the CdS NCs and CdS/ZnS NCs with and without cocatalysts. Reproduced with permission.[26] Copyright 2013, American Chemical Society.

irradiation, which was about three times as large as that of parent CdS or two times of that of parent Bi_2S_3.[61] The enhancement of photoreduction CO_2 efficiency was mainly attributed to the improvement of the separation of photoinduced charge carries and the prolongation the lifetime of photocarriers caused by the built-in energy potential. As shown in Figure 1b–e, Bi_2S_3/CdS heterostructure also exhibited superior efficiency for photodegradation of methyl red (MR).[62] Although both the photogenerated charge carries transfer from CdS to Bi_2S_3 through the interface, the difference between the migration rates of electrons and holes leads to efficient separation of the charge carriers at the interface. Moreover, the unique configuration of the Bi_2S_3 nanowire/CdS nanoparticle allows both the charge carriers to expose to the liquid phase and effectively involve in the photocatalytic reactions, resulting in the improvement of photocatalytic activity. For the bare CdS NCs, photoexcited carriers very easily transfer to the surface-trap states typically located within the semiconductor bandgap, on which the electrons or the holes with lower energy, and were unuseful for the redox reactions.[41,63]

Compared to the island type heterostructured photocatalysts, for most the core/shell heterostructured photocatalysts (**Figure 2**a), the photogenerated electron-hole pairs near the interface of junction tend to be easily confined to the core semiconductor, which are not available for photocatalytic reactions on the shell semiconductor surface. Thus, the effective separation of the electrons and holes, and effective transfer of the electron-hole pairs from the core to the outer shell surface are still challenging issues for the application of core/shell heterostructured photocatalysts. In the case of type-I core/shell CdS/ZnS NCs,[26] most the surface-trap states of the CdS can be passivated by ZnS shell. Thus, the confined electrons and holes with high energy in the core might tunnel through the ZnS shell to the outer surface for photocatalytic reactions. The CdS/ZnS NCs therefore exhibited higher activity for H_2 production and improved photocatalytic stability than bare CdS NCs (**Figure 3**). The similar phenomenon was also observed in type-I core/shell heterojunction CdSe/CdS NCs, showing a 10-fold increase in visible-light driven ($\lambda \geq 400$ nm) photocatalytic H_2 evolution activity for CdSe/CdS NCs over CdSe core NCs alone.[64] In contrast, the shell of the inverted type-I core/shell heterostructures has a smaller band gap than the core (Figure 2b).[37] Both electrons and holes would be rationally driven to the shell by the built-in energy potential, which promotes separation of the photoexcited charge carriers and efficiently facilitates charge transfer to the shell layer surface to enhance the redox reaction. For instance, the inverted type-I In_2O_3/In_2S_3 core/shell heterostructure exhibited a good H_2 evolution rate of 61.4 μmol h^{-1} g^{-1}.[46]

3.2. Type-II Heterostructures

In type-II heterostructure band alignment (**Figure 4**), the position of CB and VB of semiconductor 1 is both higher than that of semiconductor 2, and the steps in the CB and VB go in the same direction.[65,66] The band bending at the interface of type-II heterojunction due to the difference of chemical potential between semiconductor 1 and 2 induces a built-in field, which promotes the photoexcited electrons and holes to facilely move in opposite directions, and subsequently result in an

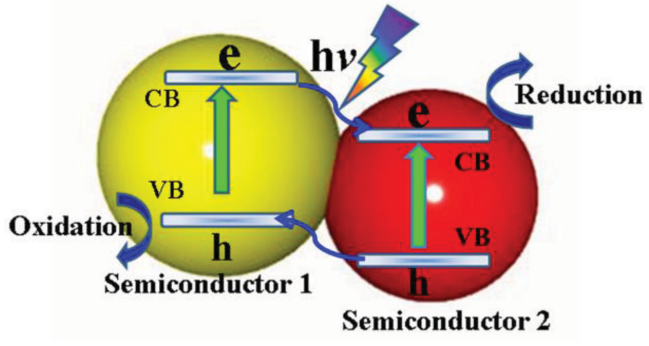

Figure 4. Schematic illustration of the type-II heterostructure band alignments, and the correspondingly possible separation and transfer process of photoinduced electron-hole pairs of semiconductor photocatalysts.

efficiently spatial separation of electron-hole pairs on different sides of heterojunction before recombination.

The narrow bandgap semiconductors were often coupled with TiO_2 to form a type-II heterostructures such as CdS/TiO_2,[67–72] WO_3/TiO_2,[73–75] Fe_2O_3/TiO_2,[76,77] AgBr/TiO_2,[78] CeO_2/TiO_2,[79] which is an effective approach to extend the photoresponse to the visible-light region. Typically, the visible-light generated electron of CdS/TiO_2 transfered from the CB of CdS to the CB of TiO_2, while the photoinduced hole of CdS remained in the VB of CdS, resulting in improvement of electron-hole separation and high efficiency for photodegradation of MB dye under visible-light irradiation.[71] The type-II In_2O_3/Ta_2O_5 heterostructure facilitated the transfer of electrons from CB of In_2O_3 to that of Ta_2O_5 and the opposite transfer route of the holes, which retarded the recombination probability of photogenerated electrons and holes. The hydrogen evolution efficiency of In_2O_3/Ta_2O_5 was about 92 μmol g^{-1} h^{-1} with a long-term stability.[80] In addition, other type-II heterostructures, such as In_2O_3/ZnO,[5] Fe_2O_3/WO_3,[81] also presented significant improvement in photocatalytic performance. More recently, ternary narrow bandgap semiconductors, such as $AgIn_5S_8$, Ag_3VO_4, and $ZnFe_2O_4$, Bi_2WO_6, and $BiVO_4$, which well match the solar spectrum, were often selected to form visible-light-driven heterostructured photocatalysts due to their large absorption coefficient.[82–85] $AgIn_5S_8/TiO_2$ heterojunction fabricated by a one-pot hydrothermal method exhibited significant improvement of the photogenerated carriers separation due to a synergistic effect of various components,[84] resulting in the enhancement of the photocatalytic H_2 production activity under visible-light illumination ($\lambda \geqq 420$ nm). Ag_3VO_4/TiO_2 nanocomposites performed high photocatalytic activities in decomposition of benzene under both visible and simulated solar light irradiation.[85] The improved photocatalytic activity of Ag_3VO_4/TiO_2 nanocomposites was originated from enhanced absorption of visible light and high efficiency of the interface charge separation. Most importantly, the excellent conversion and mineralization ratio of benzene for Ag_3VO_4/TiO_2 could be maintained for >50 h under visible light without obvious deactivation of the photocatalyst, exhibiting great photostability. CdS/$CoFe_2O_4$ and CdS/$ZnFe_2O_4$ heterostructure NCs were successfully synthesized *via* a two-step hydrothermal method.[86] Compared with pure CdS, both CdS/$ZnFe_2O_4$ and CdS/$CoFe_2O_4$ showed more broad absorption in the visible-light region and large surface area. The synergic effects of CdS and ferrites inhibited the recombination probability of photogenerated electron-hole pairs, leading to high photodegradation rate of rhodamine B (RhB) and 4-chlorophenol in aqueous solution under visible-light irradiation. In addition, photogenerated holes rapidly transferred to the solution and remained no enough holes on CdS, resulting in the remarkably photostability.

As discussed above, for the core/shell type-II heterostructured photocatalysts, one of the carriers may also suffer from being confined in the core of semiconductors, which is not easily accessible for surface reactions, instead, results in semiconductor photocorrosion. However, in the case of the outer layer with sufficiently thin and being modified with an appropriate charge-accepting moiety, the core-confined charge carriers could tunnel to the surface and be regenerated by a scavenging agent.[87] Zamkov and co-workers reported the mechanism of holes extraction from the ZnSe core to the surface of the CdS shell in a ZnSe/CdS core shell system.[88] The use of hole-scavenging surfactants was found favorable for an efficient transfer of core-localized holes to the surface even in the case of shells exceeding 7 nm in thickness. Moreover, the transfer of photoinduced electrons and holes from the core to the surface of the shell was approximately an order of magnitude faster than electron-hole recombination time, indicating that most of the absorbed energy in ZnSe/CdS could be used to drive photocatalytic reactions. For CdS/ZnSe core/shell QDs, a new energy band lower than the energy gap of both the core and shell was observed in the visible-light region. It was attributed to indirect bandgap transitions from the VB of the shell to the CB of the core, which was confirmed with steady state absorption and photoluminescence studies.[89] The interfacial electron-hole separation resulting from indirect exciton was affected by carrier trapping at interfacial defect states lying in the band offset of the CdS/ZnSe system. The indirect bandgap excitation of CdS/ZnSe reduced the hole trapping in comparison to direct bandgap excitation of CdS in the CdS/ZnSe system. The indirect-type exciton was also observed in CdTe/CdSe[90,91] and CdSe/ZnTe[90,92] core/shell QDs. The proposed indirect bandgap transition is a promising strategy to design novel nanoscale photocatalysts and effectively enhance their photocatalytic efficiency. Furthermore, the interband-gap energy states may also play a vital role in improvement of the photocatalytic reaction. The Fe_4N/Fe_2O_3 heterostructures exhibited the photosplitting of neat water into stoichiometric amounts of H_2 and O_2 under visible-light irradiation.[93] The proximity of the VB potential of the Fe_4N and Fe_2O_3 promoted the preferential transfer/entrapment of photoexcited holes. Furthermore, the defect/impurity-induced interband-gap states also led to more effective separation of electron-hole pairs, resulting in higher H_2/O_2 evolution.

As compared with particle photocatalysts, 1D nanostructures, such as nanowires,nanorods, and nanotubes, with high aspect ratio and high surface to volume ratio provide a direct pathway for charge transport and high electron mobility for efficient electronic devices. 1D TiO_2 nanostructures have become increasing importance in the application of photocatalysis originating from their superior properties in comparison with other TiO_2 nanostructured counterparts.[94] CdS/TiO_2, In_2O_3/TiO_2, and $SrTiO_3/TiO_2$ nanowire heterostructures showed high photocatalytic activity attributed to the efficient separation of photogenerated electrons and holes.[48,95–101] Other 1D heterostructures such as nanorods also show efficient photocatalytic activities. Typically, ZnO/In_2S_3 nanorod arrays showed significantly enhanced photocatalytic activity in photodegradation of RhB under visible-light irradiation,[52] resulting from the efficient separation of photoinduced charge carries and the facile charge transfer at the ZnO/In_2S_3 interface. Type-II α-Fe_2O_3/CdS nanorods showed high rate for photodegradation of MB under visible light, attributing to the synergy in visible-light absorption and charge separation at the interface of heterostructures.[102,103]

The type-II Cr-doped $SrTiO_3/TiO_2$ nanotube arrays were synthesized by hydrothermal method (**Figure 5**).[104] The photoinduced electrons of Cr-doped $SrTiO_3$ were excited from the VB (Cr 3d) to the CB (Ti 3d) and then transferred to the CB

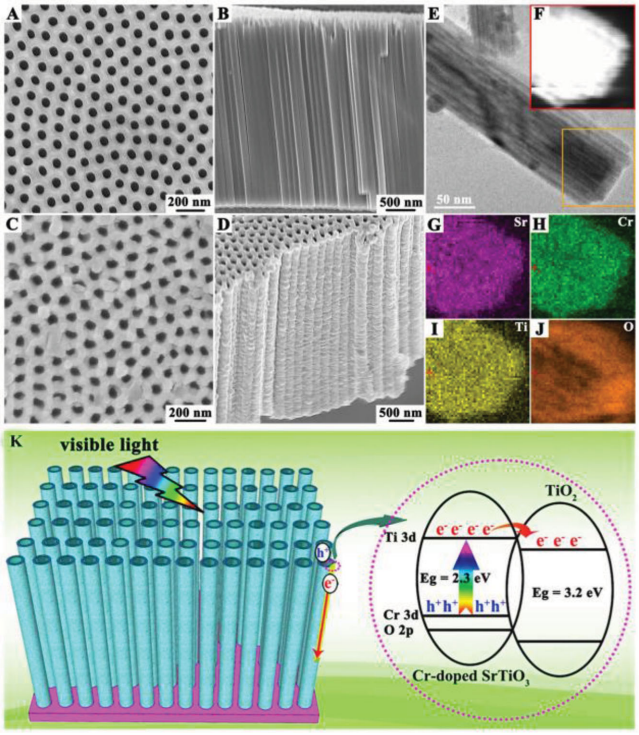

Figure 5. SEM images of A,B) TiO_2 nanotube arrays and C,D) heterostructured Cr-doped $SrTiO_3/TiO_2$ nanotube arrays treated with 1 h hydrothermal reaction times. E) TEM image, F) HAADF-STEM image, and G–J) EDX elemental mapping images of the 1 h treated Cr-doped $SrTiO_3/TiO_2$ heterostructure. K) Schematic illustration for the charge separation of Cr-doped $SrTiO_3/TiO_2$ heterostructure nanotube arrays. Reproduced with permission.[104] Copyright 2013, Nature Publishing Group.

of TiO_2, leading to enhancement of visible-light response and separation of photogenerated charge carriers. Other narrow-bandgap semiconductors couple with 1D TiO_2 nanostructures to form type-II heterostructures, including CdS/TiO_2,[99,105–113] $CdSe/TiO_2$,[114,115] and $CdTe/TiO_2$.[115] CdS QDs-sensitized TiO_2 nanotube arrays showed the high H_2 production rate of 1257 mL h^{-1} cm^{-2} under AM 1.5 illuminations, which benefited from the extended light absorption, the improved separation of photoexcited electron-hole pairs, and the facile charge-transfer properties of TiO_2 nanotube arrays.[110] Moreover, the quality of the heterojunction at the CdS or $CdTe/TiO_2$ interface has an important influence on the interfacial charge transfer.[115] It is exemplified not only by making the significant improvement in photocurrent efficiencies, but also by offering clear difference on the size-dependent electron injection efficiencies from the QDs. As a result, the enhancement in photocurrent up to 18 fold for CdSe QDs-sensitized TiO_2 nanotubes was achieved, relative to that of bare TiO_2 nanotubes. Based on the same mechanism, the type-II $ZnFe_2O_4/TiO_2$[116] heterostructures also exhibited obviously enhanced photocatalytic activity.

Among 1D ZnO-based type-II heterostructured photocatalysts, CdS-sensitized ZnO nanorods showed high photocurrent density (15.8 mA cm^{-2}), and their monochromatic incident photon-to-electron conversion efficiency (IPCE) was larger than 50% under the illumination of 380–520 nm light, indicating a high visible-light-driven photoelectrochemical hydrogen production capacity.[117–119] With regard to the type-II ZnO/CdTe heterojunction,[120–123] the monolayer deposition of CdTe QDs was beneficial for fast and efficient transfer of the photogenerated electrons from CdTe to ZnO nanowires, leading to effective suppression of anodic decomposition/corrosion and obvious improvement of stability. The maximum photoconversion efficiency (1.83%) for ZnO/CdTe was more than 200% higher than that of pristine ZnO nanowires.[123] Core/shell CdSe/CdS nanorod arrays were achieved by a chemical bath deposition process using hydrothermally prepared CdS nanorods as the template.[124] The absorption edge of the CdSe/CdS nanorod array was extended from 525 to 750 nm, and the corresponding photoconversion efficiency was enhanced from 0.23% (for bare CdS) to 1.6% (for CdSe/CdS), attributing to the enhanced utilization of visible light and the efficient separation of photogenerated charges at the interface.

For a multiple heterostructures, the additional heterointerfaces complicate the charge separation process compared with what happens in a single heterostructure. The visible-light-driven CdS/CdSe co-sensitized TiO_2 (TiO_2/CdS/CdSe hetrostructure) possesses a stepwise band edge structure due to the Fermi level alignment,[125,126] leading to the electric-field in the space-charge region on each side of the junction with superior ability for photoinduced charge carries separation and transfer at interface.[127] The saturated photocurrent with the TiO_2/CdS/CdSe electrode was 14.9 mA cm^{-2}, which was three times that with the TiO_2/CdS and TiO_2/CdSe photoelectrodes. The corresponding hydrogen evolution rate for TiO_2/CdS/CdSe system was further increased through passivation with deposition of a ZnS layer.[125,128] Moreover, CdS and CdSe QDs co-sensitized ZnO nanowire arrays (ZnO/CdS/CdSe) also exhibited high saturated photocurrent and high IPCE under visible-light irradiation.[129,130] With modification with $IrO_x{\bullet}nH_2O$, the photochemical stability of the ZnO/CdS/CdSe was substantially improved.[131] Furthermore, $IrO_x{\bullet}nH_2O$ could help release photogenerated holes accumulated on the surface of QDs, which suppressed electron-hole recombination and hole-induced photocorrosion of QDs. An average hydrogen evolution rate of 240 μmol h^{-1} cm^{-2} at 0.6 V vs reversible hydrogen electrode (RHE) was achieved with almost 100% of Faradic efficiency.

The adjustment of electronic band structure for heterostructured photocatalysts is a promising route to improve photocatalytic performance.[132] For the TiO_2/CdS_xSe_{1-x} core/shell nanowire arrays, the shell consists of more complex multinary phases including CdSe and CdS.[133] The unique CdS-CdSSe-CdSe multishell structures were observed in the Se-rich shell, whereas the separated CdS and CdSe phases disappeared in the S-rich shell. The Se-rich multishell presented higher photocurrent and H_2 generation rate, ascribing to the novel band alignment for efficient electron-hole separation and enhanced visible-light absorption. Furthermore, for the ZnO/CdSSe core/shell nanowire arrays, the decrease in both the lattice mismatch and the number of defect sites on the phase interface resulted in the higher photocurrent and hydrogen evolution rate than that of CdS/TiO_2.[134] The composition-graded $Zn_xCd_{1-x}Se$/ZnO core/shell nanowire arrays showed a continuous absorption edge from 2.7 eV (460 nm) to 1.77 eV (700 nm),[135] and yielded photocurrent density of ≈5.6 mA cm^{-2} under 1 sun solar light illumination at zero bias vs Ag/AgCl.

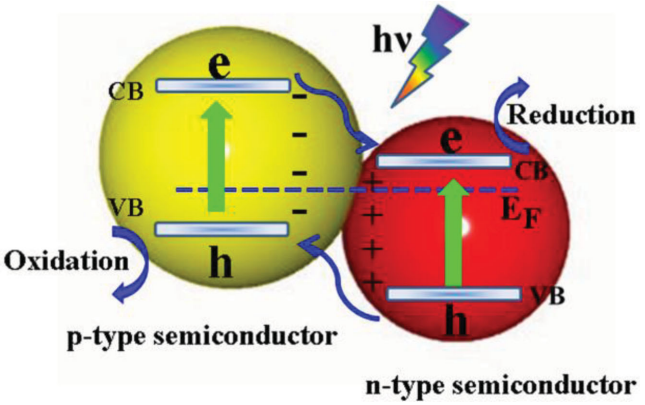

Figure 6. Schematic illustration of p–n heterostructure band alignments, and the correspondingly possible separation and transfer process of photoinduced electron-hole pairs of semiconductor photocatalysts.

3.3. p–n Heterojunctions

The design of p–n heterostructure photocatalyst systems consisting of p-type and n-type semiconductors is one of the most common methods to improve efficiency of photocatalytic reaction (**Figure 6**). With contact of p-type and n-type semiconductors each other, the bands of the semiconductors will bend and the Fermi levels will equilibrate because of the formation of a space charge region after the diffusion of electrons and holes.[8,136] Thus, the built-in electrical potential in the space charge region from n-type side to the p-type side can direct the electrons and holes to quickly travel at the opposite direction, and allow more effective separation and longer lifetime of electron-hole pairs.[137] These advantages endow the p–n type heterostructures with an enhanced photocatalytic performance.

TiO_2 were contacted with different p-type semiconductor to form p–n heterojunction photocatalysts,[138] such as $ZnFe_2O_4$/TiO_2,[139] $CuInSe_2$/TiO_2,[140] and $CuFe_2O_4$/TiO_2.[141] Typically, the narrow bandgap semiconductor $ZnFe_2O_4$ NCs were deposited in the highly ordered TiO_2 nanotube arrays to generate $ZnFe_2O_4$/TiO_2 p–n heterostructures.[139] $ZnFe_2O_4$/TiO_2 nanocomposites could absorb both UV and visible light with a band edge of 588 nm. The stronger surface photovoltage intensity of $ZnFe_2O_4$/TiO_2 was obviously observed, indicating that the charge separation efficiency was enhanced as compared with that of TiO_2 in the UV light region, due to the formation of a p–n heterojunction. In addition, the $ZnFe_2O_4$/TiO_2 nanocomposite also exhibited remarkably high photoelectrocatalytic stability with little loss even after five cycles. Similar enhancement of the photocatalytic activity of ZnO-based nanocomposites with p-type semiconductors (including NiO,[142] $CuInSe_2$,[143] $CuInS_2$,[143] CuO,[144–146] Cu_2O[147,148] were also observed.

However, the utilization of visible light is still quite low in TiO_2- and ZnO-based p–n heterostructure photocatalysts because of the large bandgaps of TiO_2 and ZnO. Thus, it is necessary to synthesize p–n heterojunction consisting of two narrow bandgap semiconductors with high activity under a wide range of visible-light irradiation. The MoS_2/CdS p–n heterojunction exhibited an optimal photocurrent of 28 mA cm^{-2} and high IPCE of approximately 28% at 420 nm at 0 V vs Ag/AgCl,[149] and the theoretical rate of H_2 evolution was calculated to be 523.1 μmol cm^{-2} h^{-1}. The high photoelectrocatalytic activity and stability of MoS_2/CdS toward the water splitting were attributed not only to the visible light absorption but also to the efficient separation of photoinduced carriers by the internal electrostatic field in the p–n junction region. The CuO/In_2O_3 heterojunction displayed the enhanced photocatalytic activity and stability even at wavelengths longer than 650 nm for effective photodegradation of RhB.[150] Other p–n heterostructures, such as Co_3O_4/$BiVO_4$,[151,152] Ag_3PO_4/$BiVO_4$,[153] $CaFe_2O_4$/TaON,[154] also showed high photocatalytic performance.

Additionally, n-p–n type heterojunction is proposed to further improve photocatalytic activities. Tang and co-workers fabricated highly efficient core/shell ZnO/TiO_2 n-p–n heterojunction nanorods.[155] In this system, two inner electric fields were formed between n-type ZnO and p-type Zn^{2+}-doped Ti_2O_3, and between p-type Zn^{2+} -doped Ti_2O_3 and n-type TiO_2. Numerous oxygen vacancies binding electrons were resulted from the replacement of Ti^{3+} by Zn^{2+} in the interface region (i.e., Zn^{2+}-doped Ti_2O_3), leading to an exciton energy level near the bottom of the CB of Ti_2O_3, lower than that of TiO_2. Due to the two inner electric fields, the photoinduced electrons in ZnO and TiO_2 transferred to the CB of Zn^{2+}-doped Ti_2O_3, significantly promoting the separation of electron-hole pairs. Therefore, the photodegradation rate of methyl orange (MO) for ZnO/TiO_2 n-p–n heterojunction nanorods was around fourfold and threefold compared to those for the P25 and bare ZnO nanorods at the same irradiation time, respectively.

3.4. Homojunction Systems

The homojunction is the junction layers made of same semiconductor materials. The difference in the positions of band edges between two sides of homojunction could build an internal field and thus facilely suppress the photoinduced electron-hole recombination. Moreover, the fact that the same composition on both sides of the interface in the homojunction region provides continuity of the band bonding, which facilitates the photogenerated charge carriers transfer across the interface. Therefore, the homojunction provides a new mechanism for the efficient separation of photoinduced charge carriers and enhancement of the photocatalytic performance.[156–163] A hierarchical TiO_2 nanostructure photoelectrode with a core/shell structure was synthesized, of which the core portion was rutile TiO_2 nanodendrite arrays and the shell portion was rutile and anatase TiO_2 NCs.[158] The TiO_2 nanodendrite arrays provided a fast electron transport pathway, and the shell portion endows a larger surface area for more efficient photoinduced electron-hole separation without significantly sacrificing the electron collection efficiency. The anatase/rutile TiO_2 homojunction enhanced the charge separation as the CB edge of anatase TiO_2 is higher than that of rutile TiO_2. A homojunction between α-Bi_2O_3 and γ-Bi_2O_3 composites exhibited higher photocatalytic activity than bare α-Bi_2O_3 or γ-Bi_2O_3 in the photodegradation of RhB, which was attributed to the synergetic effect of the homojunction.[164] The type-II tailored α/β phase Ga_2O_3 homojunction also presented significantly enhanced photocatalytic

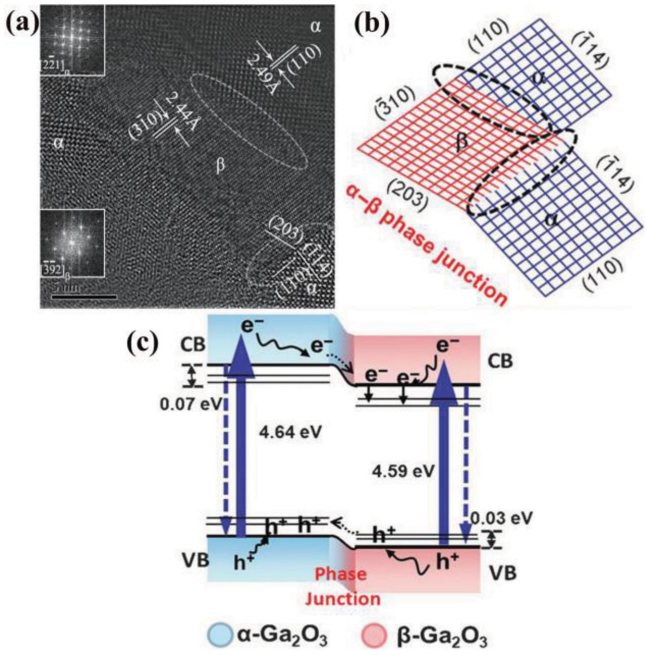

Figure 7. a) HRTEM image of Ga_2O_3. b) A simplified cartoon depicting the α-β phase junctions according to (a). c) Illustration of charge transfer cross the α-β phase junction. Reproduced with permission.[165] Copyright 2012, John Wiley & Sons, Inc.

activity for water splitting than those with α or β phase structures alone (**Figure 7**).[165] Although the potential difference caused by the differing band levels of α-Ga_2O_3 and β-Ga_2O_3 is small (The CB and VB offset between α-Ga_2O_3 and β-Ga_2O_3 were ~0.07 eV and ~0.03 eV, respectively), the photoinduced electrons can still transfer from the α-phase to the β-phase, and the photogenerated holes can move from the β-phase to the α-phase, which was of great benefit for enhancing the photocatalytic reaction. A cobalt-doped mixed phase/biphasic ZnO homojunction with zinc blende (ZB) and wurtzite (WZ) phases showed high visible-light-induced photodegradation of MB and phenol due to favorable charge separation and transport characteristics of the interface.[166] The band gap of Bi_2WO_6 QDs in the Bi_2WO_6 QDs/Bi_2WO_6 nanosheets homojunction was widened, forming type-I staggered band alignment.[167] Under visible-light irradiation, the photogenerated electrons in the CB and the holes in the VB of Bi_2WO_6 QDs migrated to the CB and the VB of Bi_2WO_6 nanosheets, respectively, to inhibit the electron-hole recombination. Hence, the photocatalytic efficiency of the Bi_2WO_6 QDs/nanosheets homojunction was six times higher than that of NC-assembling Bi_2WO_6 and three times higher than that of nanoplate-assembling Bi_2WO_6, respectively.

A p–n homojunction in the same material can also be used for enhancement of photocatalytic activity. A 20 nm film of p-type Mg-doped Fe_2O_3 was deposited on n-type Fe_2O_3 by atomic layer deposition to form p–n homojunction.[168] The fast decay of open circuit voltage for p–n Fe_2O_3 indicates the effective carrier separation, attributing to the built-in internal fields. Besides doping, the dominate charge carrier type in a semiconductor can also be tunable with the solution pH, e.g. from n-type to p-type through changing acid to alkaline solutions.[169–172] The p-Cu_2O (pH = 9)/n-Cu_2O (pH = 4.9) homojunction displayed large interfacial electric field and high charge separation efficiency, resulting in highly photocatalytic reduction of methylviologen (MV^{2+}).[170]

More importantly, it is possible to achieve high charge separation efficiency via construction of a large magnitude of interfacial electric field within a semiconductor. A gradient W-doped $BiVO_4$ homojunction photoanode was prepared by spray pyrolysis.[173] A distributed n^+–n homojunction in $BiVO_4$ was created through introduction of a gradient dopant concentration in the dopant profile, which greatly enhanced the charge-separation efficiency throughout the bulk of the material rather than just at the interface. Therefore, the carrier-separation efficiency of gradient W-doped $BiVO_4$ photoanode up to 80% was achieved. A free standing Pt/n-Si/n^+-Si/Ag heterostructure nanowire, which was encased in a silica insulating shell, exhibited excellent activity in dye photodegradation reactions (**Figure 8**).[174] This system facilitated efficient separation of electron-hole pairs. Meanwhile, the 1D morphology and insulating shell enable the separated electrons and holes to transfer in opposite directions toward two metal catalysts for the desired reactions. Moreover, the insulating shell reduced direct photoelectrochemical reactions on the semiconductor surface, and therefore minimized the semiconductor photodegradation, which ensures the electrochemical stability of the whole system.

The twin-induced $Cd_{0.5}Zn_{0.5}S$ nanorods consisting of alternating ZB and WZ segments along <111> direction led to the generation of series of homojunctions with short spacing in a specific dimension (**Figure 9**).[175] The up-shift of both CB and

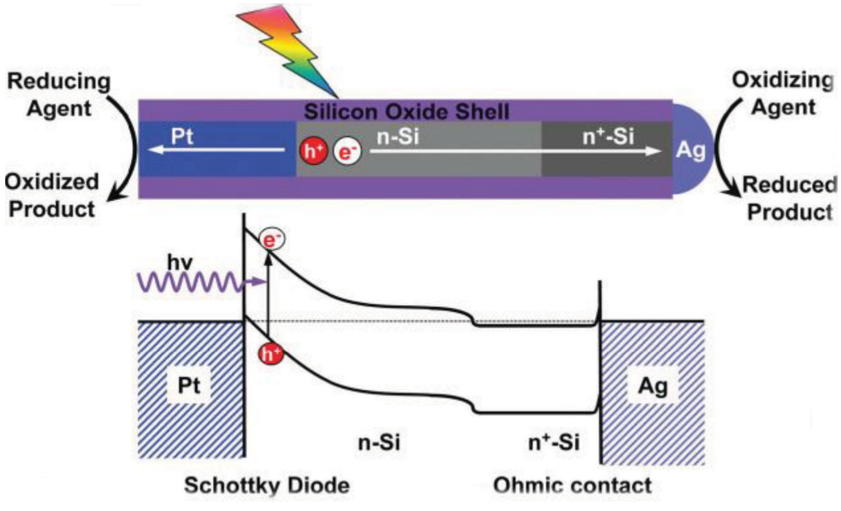

Figure 8. Schematic illustration and band diagram of Pt/n-Si/n^+-Si/Ag photocatalyst. The photoexcited electron-hole pairs quickly dissociate into separated electrons and holes, which migrate in opposite directions toward the two ends for the desired reduction reaction on Ag and the oxidation reaction on Pt, respectively. Reproduced with permission.[174] Copyright 2010, American Chemical Society.

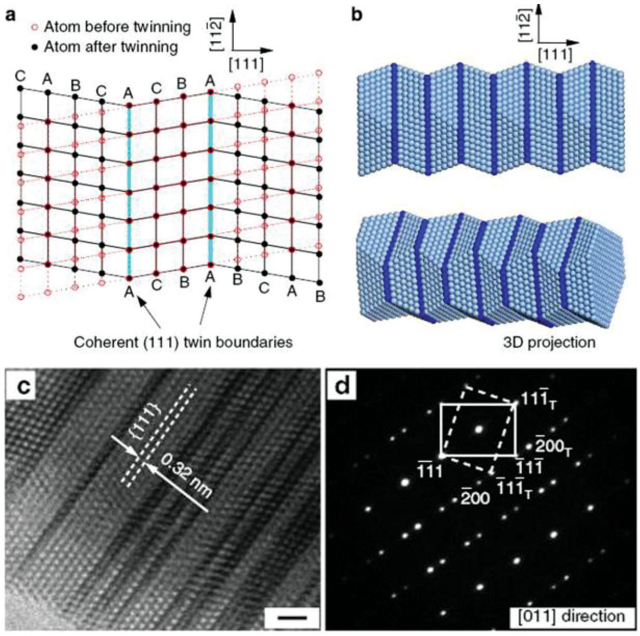

Figure 9. Structural models of a typical twinned $Cd_{0.5}Zn_{0.5}S$. a) Two (111)/[11–2] type coherent twin planes involve in a zinc blende FCC lattice matrix. The thicker cyan lines represente twin planes. Red circles and solid black solid are lattice configurations before and after twining, respectively. b) A twinned $Cd_{0.5}Zn_{0.5}S$ nanorod as seen from the [-110] direction, and three-dimensional projection as observed from a high-index [-hhk] direction (The dark blue layers indicated the twin planes). c) HRTEM of the twinned $Cd_{0.5}Zn_{0.5}S$ nanorod with {111} twin plane (scale bars is 1 nm). d) The selected area electron diffraction (SAED) patterns confirme the formation of (111)/[11–2]-type slips in nano-twins of $Cd_{0.5}Zn_{0.5}S$. Reproduced with permission.[175] Copyright 2013, Nature Publishing Group.

VB energy levels for WZ segments compared with that of ZB segments could simultaneously lead to efficient separation of photoexcited electrons and holes. It was obviously different from most of heterojunctions that can only separate either electrons or holes alone. Furthermore, large distribution and the close interconnection at the atomic level of two phases (ZB and WZ) in such homojunctions were beneficial for the vectorial transfer of photoinduced charges. In addition, $Cd_{0.5}Zn_{0.5}S$ NCs with nano-twin structures also exhibited high activity for hydrogen evolution from water under visible-light irradiation ($\lambda \geqq 430$ nm) without noble metals, with an extremely high apparent quantum yield of 43% at 425 nm.[176] The "back to back" potential (twin-boundary-dependent potential) formed by parallel nano-twins in the $Cd_{1-x}Zn_xS$ crystals significantly improves the separation of the photogenerated electron-hole pairs, and subsequently leads to enhancement of the photocatalytic activity.[176]

3.5. Z-Scheme Systems

In the development of visible-light-driven photocatalytic systems, Z-scheme was originally introduced by Bard in 1979, which was driven by a two-step photoexcitation.[177] The Z-scheme is generally composed of a H_2-evolving photocatalyst, an O_2-evolving photocatalyst, and an electron mediator.[8,9,178]

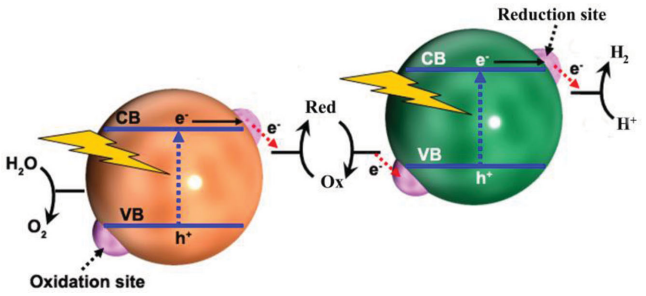

Figure 10. Schematic illustrations of the Z-scheme in the presence of IO^{3-}/I^- as electron mediators, Red and Ox indicate electron donating and accepting species, respectively.

The Z-scheme photocatalysis system allows overall water splitting. The principal advantage of the Z-scheme lies in the availability of the strongly reductive electrons of one photocatalyst and the strongly oxidative holes of the other. The Z-scheme system has been applied for water splitting,[179–184] CO_2 photoreduction,[185,186] and photodegradation or oxidation of organic contaminants.[187,188]

Several semiconductor-based Z-scheme systems consisting of two isolated photocatalysts and the redox mediators (Ox/Red) (e.g. IO^{3-}/I^-, and Fe^{3+}/Fe^{2+}) have been well developed, which are active for splitting water into H_2 and O_2,[178,181,184,189–192] as shown in **Figure 10**. Domen and co-workers achieved the construction of Z-scheme system using IO^{3-}/I^- as redox mediators, $Pt/SrTiO_3$:Cr, Ta as a H_2-evolving photocatalyst, and Pt/WO_3 as an O_2-evolving photocatalyst.[189] The Z-scheme systems consisting of $Pt/SrTiO_3$:Rh as a H_2-evolving photocatalyst, and O_2-evolving photocatalysts such as $BiVO_4$, Bi_2MoO_6, and WO_3 were also achieved in the presence of Fe^{3+}/Fe^{2+} redox couple, resulting in the achievement of production of H_2 and O_2.[191]

Nevertheless, this Z-scheme photocatalytic system has various negative effects, such as back reactions for water splitting reaction.[119] The redox mediators also strongly absorb the visible light, reducing the light absorption of semiconductor photocatalysts. Thus, the all-solid-state Z-scheme systems were greatly developed in recent years. The noble-metale particles (such as Au, Ag) were explored as an electron mediator for the Z-scheme system (**Figure 11**a),[193–199] providing insight into the design of novel and highly efficient Z-scheme visible-light photocatalysts. Tada and co-workers fabricated an all-solid-state Z-scheme $CdS/Au/TiO_2$ by a simple photochemical technique.[196] Under UV irradiation, the photoexcited electrons in CB of TiO_2 transferred to Au and then to the VB of CdS, and subsequently recombined with holes photogenerated in CdS. Simultaneously, the photogenerated electrons in CB of CdS and holes in the VB of TiO_2 exhibited strong reduction power and oxidation power, respectively, leading to high photocatalytic reduction of methylviologen (MV^{2+}). Moreover, the photoexcited holes in VB of CdS were recombined with electrons from TiO_2, resulting in the improvement of photostability of CdS. The photocatalytic activity of CdS/Au/ZnO Z-scheme system was also improved due to more facile electron transfer from ZnO to CdS mediated by Au.[200] Recently, Yun and co-workers reported a combination of two visible-light sensitive Z-scheme photocatalysts $CdS/Au/TiO_{1.96}C_{0.04}$.[194] Photogenerated electrons at

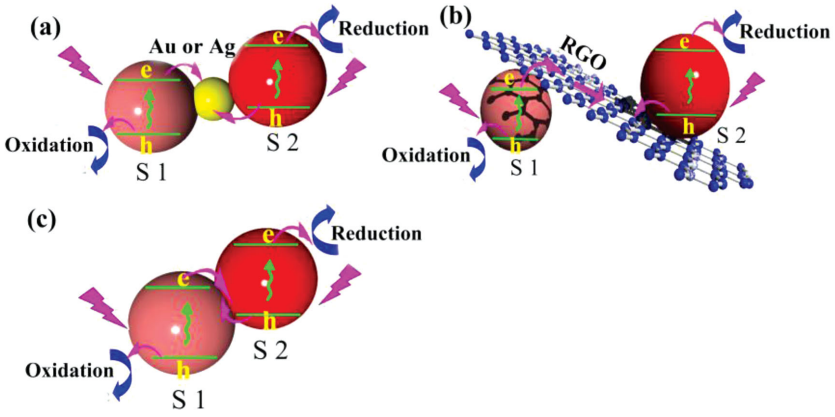

Figure 11. a) Schematic illustrations of the Z-scheme in the presence of Au, Ag as electron-mediators. b) Schematic illustrations of the Z-scheme in the presence of RGO as electron-mediators. c) Schematic illustrations of the direct Z-scheme, S1:semiconductor 1; S2:semiconductor 2.

$TiO_{1.96}C_{0.04}$ under the visible-light irradiation transferred to CdS through the Au, resulting in a decrease in the probability of electron-hole recombination at CdS. Thus a higher amount of photogenerated electrons at CdS were available to participate in the reduction reaction, leading to an exceptional performance in the photocatalytic evolution of H_2. Additionally, the Z-scheme system of $AgBr/Ag/Bi_2WO_6$ exhibited higher photodegradation rates of organic pollutants than AgBr and Bi_2WO_6 due to the low recombination rates of the photoinduced electron-hole pairs mediated by Ag.[198] A study claimed that visible-light driven $WO_3/W/PbBi_2Nb_{1.9}Ti_{0.1}O_9$ photocatalysts could also follow the Z-scheme mechanism.[197] The electrons photoexcited in the CB of WO_3 would migrate to W and recombine with the photogenerated holes from $PbBi_2Nb_{1.9}Ti_{0.1}O_9$. Therefore, the photogenerated electrons in $PbBi_2Nb_{1.9}Ti_{0.1}O_9$ functioned for the reduction of H_2O to H_2, and the photogenerated holes in WO_3 worked for the oxidation of H_2O to O_2. Furthermore, Amal and co-workers reported that reduced graphene oxide (RGO) can also be used as a solid-state electron mediator for Z-scheme water splitting consisting of $Ru/SrTiO_3$:Rh (H_2-evolving photocatalyst) and $BiVO_4$ (O_2-evolving photocatalyst) (Figure 11b).[201] In this system, the best balance between the extent of RGO reduction and the hydrophobicity was a crucial factor in enhancement of photocatalytic efficiency, due to the efficient transfer of photoexcited electrons from $BiVO_4$ to $Ru/SrTiO_3$:Rh.

Recently, a so-called direct Z-scheme system without the redox mediator was also explored (Figure 11c).[183,202–204] The photoexcited electrons in one photocatalyst with a lower CB minimum could recombine with the holes in the other photocatalyst with a higher VB maximum at the solid heterostructure interface, and thus more oxidative holes and reductive electrons can be retained on different counterparts, which enhanced photocatalytic efficiency. ZnO/CdS heterostructures based on the Z-scheme mechanism were demonstrated to be highly active photocatalysts for H_2 evolution under simulated solar light irradiation.[202] The decay lifetime of carriers in the $(ZnO)_1/(CdS)_{0.2}$ heterostructure was greatly prolonged to 220 ns, indicating that the transfer of photoexcited electrons from CB of ZnO to VB of CdS retarded the recombination probability of electron-hole pairs. Thus $(ZnO)_1/(CdS)_{0.2}$ shows the H_2 evolution rate of 1805 μmol h^{-1} g^{-1}, which was 14 and 40 times as high as that of the referred CdS and ZnO photocatalysts, respectively.

As discussed above, the built-in electric field in the p–n heterojunctions leads to more effective separation and longer lifetime of the charge carriers, and a separation of reduction and oxidation reactions in nanospace.[137] These advantages are also obtained in p–n type Z-scheme photocatalysts. The p–n type Z-scheme $CaFe_2O_4/WO_3$ heterostructure NCs were synthesized by a heterogeneous nucleation process under controlled hydrothermal treatment.[204] Photogenerated electrons with a high reduction potential in the CB of $CaFe_2O_4$ reacted with oxygen molecules in air, while photogenerated holes with high oxidation power in the VB of WO_3 reacted with acetaldehyde molecules, leading to a relatively rapid decomposition of gaseous acetaldehyde under visible-light irradiation. A similar strategy was employed for photoconversion of CO_2, such as the CuO/TiO_2 Z-scheme photocatalysts.[203] The photoexcited electrons in the CB of CuO worked for the photoreduction of CO_2 into methyl formate with the formation rate of 1600 μmol h^{-1} g^{-1}, and the photogenerated holes in the VB of TiO_2 were consumed by methanol as sacrificial reagent.

4. Challenges and Perspectives

Photocatalysis appears to be a promising avenue to solve environmental and energy issues in the future. Although the photocatalytic processes involve a complicated sequence of multiple synergistic or competing steps, the efficient utilization of solar energy (especial visible-light energy) and improvement in separation and transportation of charge carriers are the main challenges and current trend to design highly effective photocatalysts. A variety of strategies, such as doping, textural modification, formation of metal/semiconductor, carbon group/semiconductor, and semiconductor/semiconductor heterojunctions were explored to enhance the efficiencies of photocatalytic activities. The construction of a semiconductor/semiconductor heterojunction demonstrates its perfect photocatalytic effectiveness through utilization of sunlight, improvement of the separation/transportation of the photogenerated electron-hole pairs, and creation of sufficient built-in potential for redox reactions. Among diverse semiconductor/semiconductor heterostructured photocatalysts, while type-I heterostructured photocatalysts present high efficiency of photocatalytic activity, however, both the photogenerated electrons and holes of one semiconductor may transfer to another semiconductor due to straddling band alignment, which is not helpful to more efficiently inhibit the electron-hole recombination. The photoexcited electrons and holes in type-II heterostructured photocatalysts facilely transfer to the opposite sides of heterojunction before recombination, which have more opportunities for separation. In despite of some shortcomings in enhancement of light absorption, the

same composition on both sides of the homojunction region provides continuity of the band bonding, which facilitates the photogenerated charge carriers transfer across the interface, resulting in enhancement of the photocatalytic performance. As compared with non-p–n heterostructured photocatalysts (type-I heterojunctions, type-II heterojunctions, and homojunctions), the built-in electrical potential in the space charge region from n-type side to the p-type side can direct the electrons and holes to quickly travel at the opposite direction, and allow more effective separation and longer lifetime of electron-hole pairs. However, for above-mentioned heterostructured photocatalysts, one clear drawback is that the redox ability of transferred electrons and holes is weakened by the release of a portion of the potential energy. In contrast, Z-scheme-based heterostructured photocatalysts simultaneously possess high charge-separation and strong oxidative holes and reductive electrons, which were isolated on different semiconductors. The electron mediator of Z-scheme photocatalysts plays an important role in charge carrier transportation. All-solid-state Z-scheme photocatalysts eliminate various negative effects of solution-based Z-scheme systems, such as back reactions. Although the solar-light conversion efficiency is still low at the present stage, Z-scheme photocatalysts may be the most promising photocatalytic systems.

Although great progresses have been achieved in investigation of heterostructured photocatalytsts, it is still some challenges to design high efficiency of photocatalytic systems. Firstly, there is no a detail understanding of the charge generation, separation and transportation across nanoscale interfaces of heterostructured photocatalysts, which are critical for the design and optimization of highly efficient photocatalysts. Secondly, while most available photocatalysts so far can only function in the UV or near UV regime, the highly effective utilization of visible light is another challenge of heterostructured photocatalysts. Finally, photostability of heterostructured photocatalytst is and will still be one main challenge for practical applications. Therefore, the deepening knowledge of the photocatalytic mechanism and exploration of new materials are indispensible to make substantial breakthroughs for practical application of photocatalysts.

Acknowledgements

This work was supported by 973 Programs (No. 2014CB239302, 2011CB933303, and 2013CB632404), National Natural Science Foundation of China (No. 21473091, 51272101, and 51202005), National Science Foundation of Jiangsu Province (No. BK2012015 and BK 20130053), and College Postgraduate Research and Innovation Project of Jiangsu Province (No. CXZZ13_0033), Provincial Science Key Foundation of Higher Education Institutions of Anhui (No. KJ2011A053), China Postdoctoral Science Foundation (No. 2012M521037).

Received: May 20, 2014
Revised: September 19, 2014
Published online: January 7, 2015

[1] Z. G. Zou, J. H. Ye, K. Sayama, H. Arakawa, *Nature* **2001**, *414*, 625.
[2] M. G. Walter, E. L. Warren, J. R. McKone, S. W. Boettcher, Q. X. Mi, E. A. Santori, N. S. Lewis, *Chem. Rev.* **2010**, *110*, 6446.
[3] S. N. Habisreutinger, L. Schmidt-Mende, J. K. Stolarczyk, *Angew. Chem. Int. Ed.* **2013**, *52*, 7372.
[4] Q. Liu, Y. Zhou, J. H. Kou, X. Y. Chen, Z. P. Tian, J. Gao, S. C. Yan, Z. G. Zou, *J. Am. Chem. Soc.* **2010**, *132*, 14385.
[5] W. G. Tu, Y. Zhou, Q. Liu, S. C. Yan, S. S. Bao, X. Y. Wang, M. Xiao, Z. G. Zou, *Adv. Funct. Mater.* **2013**, *23*, 1743.
[6] J. S. Lee, K. H. You, C. B. Park, *Adv. Mater.* **2012**, *24*, 1084.
[7] M. S. Zhu, P. L. Chen, M. H. Liu, *ACS Nano* **2011**, *5*, 4529.
[8] W. Fan, Q. Zhang, Y. Wang, *Phys. Chem. Chem. Phys.* **2013**, *15*, 2632.
[9] Y. Q. Qu, X. F. Duan, *Chem. Soc. Rev.* **2013**, *42*, 2568.
[10] A. Fujishima, K. Honda, *Nature* **1972**, *238*, 37.
[11] G. Wang, B. Huang, X. Ma, Z. Wang, X. Qin, X. Zhang, Y. Dai, M. H. Whangbo, *Angew. Chem. Int. Ed.* **2013**, *52*, 4810.
[12] R. G. Li, F. X. Zhang, D. G. Wang, J. X. Yang, M. R. Li, J. Zhu, X. Zhou, H. X. Han, C. Li, *Nat. Commun.* **2013**, *4*, 1432.
[13] X. B. Chen, Y. B. Lou, A. C. S. Samia, C. Burda, J. L. Gole, *Adv. Funct. Mater.* **2005**, *15*, 41.
[14] X. W. Zhang, T. Zhang, J. Ng, D. D. Sun, *Adv. Funct. Mater.* **2009**, *19*, 3731.
[15] J. Tian, Z. Zhao, A. Kumar, R. I. Boughton, H. Liu, *Chem. Soc. Rev.* **2014**, *43*,6920.
[16] C. T. Dinh, H. Yen, F. Kleitz, T. O. Do, *Angew. Chem.* **2014**, *53*, 6618.
[17] W. Zhou, G. Du, P. Hu, Y. Yin, J. Li, J. Yu, G. Wang, J. Wang, H. Liu, J. Wang, H. Zhang, *J. Hazard. Mater.* **2011**, *197*, 19.
[18] L. Q. Jing, W. Zhou, G. H. Tian, H. G. Fu, *Chem. Soc. Rev.* **2013**, *42*, 9509.
[19] W. G. Tu, Y. Zhou, Z. G. Zou, *Adv. Funct. Mater.* **2013**, *23*, 4996.
[20] J. Zhang, M. Zhang, R. Q. Sun, X. Wang, *Angew. Chem. Int. Ed.* **2012**, *51*, 10145.
[21] W. G. Tu, Y. Zhou, Q. Liu, Z. P. Tian, J. Gao, X. Y. Chen, H. T. Zhang, J. G. Liu, Z. G. Zou, *Adv. Funct. Mater.* **2012**, *22*, 1215.
[22] H. J. Chen, L. Shao, Q. Li, J. F. Wang, *Chem. Soc. Rev.* **2013**, *42*, 2679.
[23] H. Tada, T. Kiyonaga, S. Naya, *Chem. Soc. Rev.* **2009**, *38*, 1849.
[24] H. Tang, C. M. Hessel, J. Wang, N. Yang, R. Yu, H. Zhao, D. Wang, *Chem. Soc. Rev.* **2014**, *43*, 4281.
[25] Q. Xiang, J. Yu, M. Jaroniec, *Chem. Soc. Rev.* **2012**, *41*, 782.
[26] K. K. Manga, Y. Zhou, Y. L. Yan, K. P. Loh, *Adv. Funct. Mater.* **2009**, *19*, 3638.
[27] H. J. Li, Y. Zhou, L. Chen, W. J. Luo, Q. F. Xu, X. Y. Wang, M. Xiao, Z. G. Zou, *Nanoscale* **2013**, *5*, 11933.
[28] Y. Myung, D. M. Jang, T. K. Sung, Y. J. Sohn, G. B. Jung, Y. J. Cho, H. S. Kim, J. Park, *ACS Nano* **2010**, *4*, 3789.
[29] J. Pan, S. M. Huhne, H. Shen, L. S. Xiao, P. Born, W. Mader, S. Mathur, *J. Phys. Chem. C* **2011**, *115*, 17265.
[30] R. Zamani, R. Fiz, J. Pan, T. Fischer, S. Mathur, J. R. Morante, J. Arbiol, *CrystEngComm* **2013**, *15*, 4532.
[31] Y. Lin, Y. Xu, M. T. Mayer, Z. I. Simpson, G. McMahon, S. Zhou, D. Wang, *J. Am. Chem. Soc.* **2012**, *134*, 5508.
[32] T. Wang, Z. Luo, C. Li, J. Gong, *Chem. Soc. Rev.* **2014**, *43*,7469.
[33] S. M. George, *Chem. Rev.* **2010**, *110*, 111.
[34] G. N. Parsons, S. M. George, M. Knez, *MRS Bull.* **2011**, *36*, 865.
[35] J. Park, J. Joo, S. G. Kwon, Y. Jang, T. Hyeon, *Angew. Chem. Int. Ed.* **2007**, *46*, 4630.
[36] Y. Yin, A. P. Alivisatos, *Nature* **2005**, *437*, 664.
[37] P. Reiss, M. Protiere, L. Li, *Small* **2009**, *5*, 154.
[38] N. N. Hewa-Kasakarage, P. Z. El-Khoury, A. N. Tarnovsky, M. Kirsanova, I. Nemitz, A. Nemchinov, M. Zamkov, *ACS Nano* **2010**, *4*, 1837.
[39] W. K. Bae, K. Char, H. Hur, S. Lee, *Chem. Mater.* **2008**, *20*, 531.
[40] P. Reiss, J. Bleuse, A. Pron, *Nano Lett.* **2002**, *2*, 781.
[41] L. Huang, X. L. Wang, J. H. Yang, G. Liu, J. F. Han, C. Li, *J. Phys. Chem. C* **2013**, *117*, 11584.

[42] J. S. Steckel, J. P. Zimmer, S. Coe-Sullivan, N. E. Stott, V. Bulovic, M. G. Bawendi, *Angew. Chem. Int. Ed.* **2004**, *43*, 2154.
[43] D. A. Chen, F. Zhao, H. Qi, M. Rutherford, X. G. Peng, *Chem. Mater.* **2010**, *22*, 1437.
[44] H. M. Zhu, N. H. Song, T. Q. Lian, *J. Am. Chem. Soc.* **2010**, *132*, 15038.
[45] Y. Ghosh, B. D. Mangum, J. L. Casson, D. J. Williams, H. Htoon, J. A. Hollingsworth, *J. Am. Chem. Soc.* **2012**, *134*, 9634.
[46] X. Yang, J. Xu, T. Wong, Q. Yang, C. S. Lee, *Phys. Chem. Chem. Phys.* **2013**, *15*, 12688.
[47] Z. Fang, Y. Liu, Y. Fan, Y. Ni, X. Wei, K. Tang, J. Shen, Y. Chen, *J. Phys. Chem. C* **2011**, *115*, 13968.
[48] S. Q. Liu, N. Zhang, Z. R. Tang, Y. J. Xu, *ACS Appl. Mater. Interfaces* **2012**, *4*, 6378
[49] D. H. Son, S. M. Hughes, Y. D. Yin, A. P. Alivisatos, *Science* **2004**, *306*, 1009.
[50] J. B. Rivest, P. K. Jain, *Chem. Soc. Rev.* **2013**, *42*, 89.
[51] B. J. Beberwyck, Y. Surendranath, A. P. Alivisatos, *J. Phys. Chem. C* **2013**, *117*, 19759.
[52] S. Khanchandani, S. Kundu, A. Patra, A. K. Ganguli, *J. Phys. Chem. C* **2013**, *117*, 5558.
[53] V. Etacheri, M. K. Seery, S. J. Hinder, S. C. Pillai, *Chem. Mater.* **2010**, *22*, 3843.
[54] L. Li, Y. L. Zhang, A. M. Schultz, X. Liu, P. A. Salvador, G. S. Rohrer, *Catal. Sci. Technol.* **2012**, *2*, 1945.
[55] V. Luca, M. G. Blackford, K. S. Finnie, P. J. Evans, M. James, M. J. Lindsay, M. Skyllas-Kazacos, P. R. F. Barnes, *J. Phys. Chem. C* **2007**, *111*, 18479.
[56] C. Z. Yao, B. H. Wei, L. X. Meng, H. Li, Q. J. Gong, H. Sun, H. X. Ma, X. H. Hu, *J. Power. Sources* **2012**, *207*, 222.
[57] A. L. Linsebigler, G. Q. Lu, J. T. Yates, *Chem. Rev.* **1995**, *95*, 735.
[58] Y. Wang, Q. Wang, X. Zhan, F. Wang, M. Safdar, J. He, *Nanoscale* **2013**, *5*, 8326.
[59] T. Teranishi, M. Sakamoto, *J. Phys. Chem. Lett.* **2013**, *4*, 2867.
[60] J. Su, X. X. Zou, G. D. Li, X. Wei, C. Yan, Y. N. Wang, J. Zhao, L. J. Zhou, J. S. Chen, *J. Phys. Chem. C* **2011**, *115*, 8064.
[61] X. Li, J. T. Chen, H. L. Li, J. T. Li, Y. T. Xu, Y. J. Liu, J. R. Zhou, *J. Nat. Gas. Chem.* **2011**, *20*, 413.
[62] Z. Fang, Y. F. Liu, Y. T. Fan, Y. H. Ni, X. W. Wei, K. B. Tang, J. M. Shen, Y. Chen, *J. Phys. Chem. C* **2011**, *115*, 13968.
[63] L. Huang, J. H. Yang, X. l. Wang, J. Han, H. X. Han, C. Li, *Phys. Chem. Chem. Phys.* **2013**, *15*, 553.
[64] A. Thibert, F. A. Frame, E. Busby, M. A. Holmes, F. E. Osterloh, D. S. Larsen, *J. Phys. Chem. Lett.* **2011**, *2*, 2688.
[65] R. Marschall, *Adv. Funct. Mater.* **2014**, *24*, 2421.
[66] S. S. Lo, T. Mirkovic, C. H. Chuang, C. Burda, G. D. Scholes, *Adv. Mater.* **2011**, *23*, 180.
[67] Y. Bessekhouad, D. Robert, J. Weber, *J. Photoch. Photobio. A* **2004**, *163*, 569.
[68] J. C. Yu, L. Wu, J. Lin, P. S. Li, Q. Li, *Chem. Commun.* **2003**, 1552.
[69] S. J. Ding, X. Yin, X. J. Lu, Y. M. Wang, F. Q. Huang, D. Y. Wan, *ACS Appl. Mater. Interfaces* **2012**, *4*, 306.
[70] J. S. Jang, S. H. Choi, H. G. Kim, J. S. Lee, *J. Phys. Chem. C* **2008**, *112*, 17200.
[71] J. Y. Wang, Z. H. Liu, Q. Zheng, Z. K. He, R. X. Cai, *Nanotechnology* **2006**, *17*, 4561.
[72] H. L. Meng, C. Cui, H. L. Shen, D. Y. Liang, Y. Z. Xue, P. G. Li, W. H. Tang, *J. Alloy. Compd.* **2012**, *527*, 30.
[73] N. A. Ramos-Delgado, L. Hinojosa-Reyes, I. L. Guzman-Mar, M. A. Gracia-Pinilla, A. Hernandez-Ramirez, *Catal. Today.* **2013**, *209*, 35.
[74] S. Y. Chai, Y. J. Kim, W. I. Lee, *J. Electroceram.* **2006**, *17*, 909.
[75] S. A. K. Leghari, S. Sajjad, J. L. Zhang, *RSC Adv.* **2013**, *3*, 15354.
[76] M. A. Ahmed, E. E. El-Katori, Z. H. Gharni, *J. Alloy. Compd.* **2013**, *553*, 19.
[77] K. E. deKrafft, C. Wang, W. B. Lin, *Adv. Mater.* **2012**, *24*, 2014.
[78] M. Abou Asi, C. He, M. H. Su, D. H. Xia, L. Lin, H. Q. Deng, Y. Xiong, R. L. Qiu, X. Z. Li, *Catal. Today.* **2011**, *175*, 256.
[79] Y. G. Wang, B. Li, C. L. Zhang, L. F. Cui, S. F. Kang, X. Li, L. H. Zhou, *Appl. Catal. B Environ.* **2013**, *130*, 277.
[80] L. L. Xu, J. G. Guan, L. A. Gao, Z. G. Sun, *Catal. Commun.* **2011**, *12*, 548.
[81] D. Q. Bi, Y. M. Xu, *J. Mol. Catal. A Chem.* **2013**, *367*, 103.
[82] J. Tian, Y. H. Sang, G. W. Yu, H. D. Jiang, X. N. Mu, H. Liu, *Adv. Mater.* **2013**, *25*, 5075.
[83] N. Wetchakun, S. Chaiwichain, B. Inceesungyorn, K. Pingmuang, S. Phanichphant, A. I. Minett, J. Chen, *ACS Appl. Mater. Interfaces* **2012**, *4*, 3718.
[84] K. Li, B. Chai, T. Y. Peng, J. Mao, L. Zan, *ACS Catal.* **2013**, *3*, 170.
[85] J. X. Wang, H. Ruan, W. J. Li, D. Z. Li, Y. Hu, J. Chen, Y. Shao, Y. Zheng, *J. Phys. Chem. C* **2012**, *116*, 13935.
[86] P. Xiong, J. w. Zhu, X. Wang, *Ind. Eng. Chem. Res.* **2013**, *52*, 17126.
[87] Z. J. Jiang, D. F. Kelley, *J. Phys. Chem. C* **2012**, *116*, 12958.
[88] D. Perera, R. Lorek, R. S. Khnayzer, P. Moroz, T. O'Connor, D. Khon, G. Diederich, E. Kinder, S. Lambright, F. N. Castellano, M. Zamkov, *J. Phys. Chem. C* **2012**, *116*, 22786.
[89] S. Verma, S. Kaniyankandy, H. N. Ghosh, *J. Phys. Chem. C* **2013**, *117*, 10901.
[90] S. Kim, B. Fisher, H. J. Eisler, M. Bawendi, *J. Am. Chem. Soc.* **2003**, *125*, 11466.
[91] C. D. Donega, *Phys. Rev. B* **2010**, *81*, 165303.
[92] S. Kaniyankandy, S. Rawalekar, S. Verma, H. N. Ghosh, *J. Phys. Chem. C* **2011**, *115*, 1428.
[93] P. Dhanasekaran, H. G. Salunke, N. M. Gupta, *J. Phys. Chem. C* **2012**, *116*, 12156.
[94] X. Chen, S. S. Mao, *Chem. Rev.* **2007**, *107*, 2891.
[95] T. P. Cao, Y. J. Li, C. H. Wang, C. L. Shao, Y. C. Liu, *Langmuir* **2011**, *27*, 2946.
[96] J. Zhang, J. H. Bang, C. C. Tang, P. V. Kamat, *ACS Nano* **2010**, *4*, 387.
[97] J. Ng, S. P. Xu, X. W. Zhang, H. Y. Yang, D. D. Sun, *Adv. Funct. Mater.* **2010**, *20*, 4287.
[98] H. W. Bai, Z. Y. Liu, D. D. Sun, *J. Am. Ceram. Soc.* **2013**, *96*, 942.
[99] C. L. Li, J. A. Yuan, B. Y. Han, L. Jiang, W. F. Shangguan, *Int. J. Hydrogen. Energ.* **2010**, *35*, 7073.
[100] J. B. Mu, B. Chen, M. Y. Zhang, Z. C. Guo, P. Zhang, Z. Y. Zhang, Y. Y. Sun, C. L. Shao, Y. C. Liu, *ACS Appl. Mater. Interfaces* **2012**, *4*, 424.
[101] Y. C. Chen, Y. C. Pu, Y. J. Hsu, *J. Phys. Chem. C* **2012**, *116*, 2967.
[102] Y. Shi, H. Y. Li, L. Wang, W. Shen, H. Z. Chen, *ACS Appl. Mater. Interfaces* **2012**, *4*, 4800.
[103] L. Wang, H. W. Wei, Y. J. Fan, X. Gu, J. H. Zhan, *J. Phys. Chem. C* **2009**, *113*, 14119.
[104] Z. B. Jiao, T. Chen, J. Y. Xiong, T. Wang, G. X. Lu, J. H. Ye, Y. P. Bi, *Sci. Rep.* **2013**, *3*, 2720.
[105] W. Zhu, X. Liu, H. Q. Liu, D. L. Tong, J. Y. Yang, J. Y. Peng, *J. Am. Chem. Soc.* **2010**, *132*, 12619.
[106] W. W. Zhao, Z. Y. Ma, D. Y. Yan, J. J. Xu, H. Y. Chen, *Anal. Chem.* **2012**, *84*, 10518.
[107] X. F. Gao, W. T. Sun, Z. D. Hu, G. Ai, Y. L. Zhang, S. Feng, F. Li, L. M. Peng, *J. Phys. Chem. C* **2009**, *113*, 20481.
[108] W. T. Sun, Y. Yu, H. Y. Pan, X. F. Gao, Q. Chen, L. M. Peng, *J. Am. Chem. Soc.* **2008**, *130*, 1124.
[109] H. Wang, Y. S. Bai, H. Zhang, Z. H. Zhang, J. H. Li, L. Guo, *J. Phys. Chem. C* **2010**, *114*, 16451.
[110] L. X. Sang, H. Y. Tan, X. M. Zhang, Y. T. Wu, C. F. Ma, C. Burda, *J. Phys. Chem. C* **2012**, *116*, 18633.
[111] Z. B. Shao, W. Zhu, Z. Li, Q. H. Yang, G. Z. Wang, *J. Phys. Chem. C* **2012**, *116*, 2438.

[112] Y. Xie, G. Ali, S. H. Yoo, S. O. Cho, *ACS Appl. Mater. Interfaces* **2010**, *2*, 2910.
[113] S. Banerjee, S. K. Mohapatra, P. P. Das, M. Misra, *Chem. Mater.* **2008**, *20*, 6784.
[114] J. Hensel, G. M. Wang, Y. Li, J. Z. Zhang, *Nano Lett.* **2010**, *10*, 478.
[115] H. H. Yang, W. G. Fan, A. Vaneski, A. S. Susha, W. Y. Teoh, A. L. Rogach, *Adv. Funct. Mater.* **2012**, *22*, 2821.
[116] X. Y. Li, Y. Hou, Q. D. Zhao, G. H. Chen, *Langmuir* **2011**, *27*, 3113.
[117] S. Khanchandani, S. Kundu, A. Patra, A. K. Ganguli, *J. Phys. Chem. C* **2012**, *116*, 23653.
[118] X. W. Wang, G. Liu, G. Q. Lu, H. M. Cheng, *Int. J. Hydrogen. Energ.* **2010**, *35*, 8199.
[119] Y. Y. Bu, Z. Y. Chen, W. B. Li, J. Q. Yu, *ACS Appl. Mater. Interfaces* **2013**, *5*, 5097.
[120] X. N. Wang, H. J. Zhu, Y. M. Xu, H. Wang, Y. Tao, S. Hark, X. D. Xiao, Q. A. Li, *ACS Nano* **2010**, *4*, 3302.
[121] D. Liu, Z. Z. Zheng, C. Q. Wang, Y. Q. Yin, S. Q. Liu, B. Yang, Z. H. Jiang, *J. Phys. Chem. C* **2013**, *117*, 26529.
[122] X. B. Cao, P. Chen, Y. Guo, *J. Phys. Chem. C* **2008**, *112*, 20560.
[123] H. M. Chen, C. K. Chen, Y. C. Chang, C. W. Tsai, R. S. Liu, S. F. Hu, W. S. Chang, K. H. Chen, *Angew. Chem. Int. Ed.* **2010**, *49*, 5966.
[124] M. Wang, J. G. Jiang, J. W. Shi, L. J. Guo, *Acs Appl. Mater. Interfaces* **2013**, *5*, 4021.
[125] Y. L. Lee, C. F. Chi, S. Y. Liau, *Chem. Mater.* **2010**, *22*, 922.
[126] S. L. Cheng, W. Y. Fu, B. Y. Hai, L. N. Zhang, J. W. Ma, H. Zhao, M. L. Sun, L. H. Yang, *J. Phys. Chem. C* **2012**, *116*, 2615.
[127] K. H. Lin, C. Y. Chuang, Y. Y. Lee, F. C. Li, Y. M. Chang, I. P. Liu, S. C. Chou, Y. L. Lee, *J. Phys. Chem. C* **2012**, *116*, 1550.
[128] T. Zewdu, J. N. Clifford, E. Palomares, *Phys. Chem. Chem. Phys.* **2012**, *14*, 13076.
[129] G. M. Wang, X. Y. Yang, F. Qian, J. Z. Zhang, Y. Li, *Nano Lett.* **2010**, *10*, 1088.
[130] M. Seol, H. Kim, W. Kim, K. Yong, *Electrochem. Commun.* **2010**, *12*, 1416.
[131] M. Seol, J. W. Jang, S. Cho, J. S. Lee, K. Yong, *Chem. Mater.* **2013**, *25*, 184.
[132] J. S. Luo, L. Ma, T. C. He, C. F. Ng, S. J. Wang, H. D. Sun, H. J. Fan, *J. Phys. Chem. C* **2012**, *116*, 11956.
[133] T. K. Sung, J. H. Kang, D. M. Jang, Y. Myung, G. B. Jung, H. S. Kim, C. S. Jung, Y. J. Cho, J. Park, C. L. Lee, *J. Mater. Chem.* **2011**, *21*, 4553.
[134] Y. Myung, D. M. Jang, T. K. Sung, Y. J. Sohn, G. B. Jung, Y. J. Cho, H. S. Kim, J. Park, *ACS Nano* **2010**, *4*, 3789.
[135] H. X. Li, C. W. Cheng, X. L. Li, J. P. Liu, C. Guan, Y. Y. Tay, H. J. Fan, *J. Phys. Chem. C* **2012**, *116*, 3802.
[136] L. Li, P. A. Salvador, G. S. Rohrer, *Nanoscale Res. Lett.* **2014**, *6*, 24.
[137] H. Wang, L. Zhang, Z. Chen, J. Hu, S. Li, Z. Wang, J. Liu, X. Wang, *Chem. Soc. Rev.* **2014**, *43*, 5234.
[138] D. Sarkar, C. K. Ghosh, S. Mukherjee, K. K. Chattopadhyay, *ACS Appl. Mater. Interfaces* **2013**, *5*, 331.
[139] Y. Hou, X. Y. Li, Q. D. Zhao, X. Quan, G. H. Chen, *Adv. Funct. Mater.* **2010**, *20*, 2165.
[140] Y. L. Liao, H. W. Zhang, Z. Y. Zhong, L. J. Jia, F. M. Bai, J. Li, P. Zhong, H. Chen, J. Zhang, *ACS Appl. Mater. Interfaces* **2013**, *5*, 11022.
[141] A. Kezzim, N. Nasrallah, A. Abdi, M. Trari, *Energ. Convers. Manag.* **2011**, *52*, 2800.
[142] Z. Zhang, C. Shao, X. Li, C. Wang, M. Zhang, Y. Liu, *ACS Appl. Mater. Interfaces* **2010**, *2*, 2915.
[143] F. Y. Shen, W. X. Que, Y. C. He, Y. Yuan, X. T. Yin, G. F. Wang, *Acs Appl. Mater. Inter.* **2012**, *4*, 4087.
[144] S. Jung, S. Jeon, K. Yong, *Nanotechnology* **2011**, *22*.
[145] Q. Simon, D. Barreca, A. Gasparotto, C. Maccato, T. Montini, V. Gombac, P. Fornasiero, O. I. Lebedev, S. Turner, G. Van Tendeloo, *J. Mater. Chem.* **2012**, *22*, 11739.
[146] S. Jung, K. Yong, *Chem. Commun.* **2011**, *47*, 2643.
[147] M. Deo, D. Shinde, A. Yengantiwar, J. Jog, B. Hannoyer, X. Sauvage, M. More, S. Ogale, *J. Mater. Chem.* **2012**, *22*, 17055.
[148] Y. Wang, S. C. Li, H. Shi, K. Yu, *Nanoscale* **2012**, *4*, 7817.
[149] Y. Liu, Y. X. Yu, W. D. Zhang, *J. Phys. Chem. C* **2013**, *117*, 12949.
[150] L. H. Yu, Y. Huang, G. C. Xiao, D. Z. Li, *J. Mater. Chem. A* **2013**, *1*, 9637.
[151] M. C. Long, W. M. Cai, H. Kisch, *J. Phys. Chem. C* **2008**, *112*, 548.
[152] M. Long, W. M. Cai, J. Cai, B. X. Zhou, X. Y. Chai, Y. H. Wu, *J. Phys. Chem. B* **2006**, *110*, 20211.
[153] C. Li, P. Zhang, R. Lv, J. Lu, T. Wang, S. Wang, H. Wang, J. Gong, *Small* **2013**, *9*, 3951.
[154] E. S. Kim, N. Nishimura, G. Magesh, J. Y. Kim, J. W. Jang, H. Jun, J. Kubota, K. Domen, J. S. Lee, *J. Am. Chem. Soc.* **2013**, *135*, 5375.
[155] L. Lin, Y. Yang, L. Men, X. Wang, D. He, Y. Chai, B. Zhao, S. Ghoshroy, Q. Tang, *Nanoscale* **2013**, *5*, 588.
[156] J. Zhang, X. H. Tang, D. Y. Li, *J. Phys. Chem. C* **2011**, *115*, 21529.
[157] L. G. Gai, X. Q. Duan, H. H. Jiang, Q. H. Mei, G. W. Zhou, Y. Tian, H. Liu, *CrystEngComm* **2012**, *14*, 7662.
[158] J. S. Yang, W. P. Liao, J. J. Wu, *ACS Appl. Mater. Interfaces* **2013**, *5*, 7425.
[159] Y. Luo, X. Y. Liu, J. G. Huang, *CrystEngComm* **2013**, *15*, 5586.
[160] S. F. Chen, X. L. Yu, H. Y. Zhang, W. Liu, *J. Electrochem. Soc.* **2010**, *157*, K96.
[161] S. F. Chen, W. Liu, S. J. Zhang, Y. H. Chen, *J. Sol–Gel Sci. Technol.* **2010**, *54*, 258.
[162] L. C. K. Liau, C. C. Lin, *Appl. Surf. Sci.* **2007**, *253*, 8798.
[163] J. T. Carneiro, T. J. Savenije, J. A. Moulijn, G. Mul, *J. Phys. Chem. C* **2011**, *115*, 2211.
[164] Y. Y. Sun, W. Z. Wang, L. Zhang, Z. J. Zhang, *Chem. Eng. J.* **2012**, *211*, 161.
[165] X. Wang, Q. Xu, M. R. Li, S. Shen, X. L. Wang, Y. C. Wang, Z. C. Feng, J. Y. Shi, H. X. Han, C. Li, *Angew. Chem. Int. Ed.* **2012**, *51*, 13089.
[166] B. M. Rajbongshi, S. K. Samdarshi, *Appl. Catal. B Environ.* **2014**, *144*, 435.
[167] Z. K. Cui, D. W. Zeng, T. T. Tang, J. Liu, C. S. Xie, *Catal. Commun.* **2010**, *11*, 1054.
[168] Y. J. Lin, Y. Xu, M. T. Mayer, Z. I. Simpson, G. McMahon, S. Zhou, D. W. Wang, *J. Am. Chem. Soc.* **2012**, *134*, 5508.
[169] L. C. K. Liau, Y. C. Lin, Y. J. Peng, *J. Phys. Chem. C* **2013**, *1*, 1.
[170] T. F. Jiang, T. F. Xie, W. S. Yang, L. P. Chen, H. M. Fan, D. J. Wang, *J. Phys. Chem. C* **2013**, *117*, 4619.
[171] C. M. McShane, K. S. Choi, *J. Am. Chem. Soc.* **2009**, *131*, 2561.
[172] H. M. Wei, H. B. Gong, L. Chen, M. Zi, B. Q. Cao, *J. Phys. Chem. C* **2012**, *116*, 10510.
[173] F. F. Abdi, L. H. Han, A. H. M. Smets, M. Zeman, B. Dam, R. van de Krol, *Nat. Commun.* **2013**, *4*, 2195.
[174] Y. Q. Qu, L. Liao, R. Cheng, Y. Wang, Y. C. Lin, Y. Huang, X. F. Duan, *Nano Lett.* **2010**, *10*, 1941.
[175] M. C. Liu, D. W. Jing, Z. H. Zhou, L. J. Guo, *Nat. Commun.* **2013**, *4*, 2278.
[176] M. C. Liu, L. Z. Wang, G. Q. Lu, X. D. Yao, L. J. Guo, *Energ. Environ. Sci.* **2011**, *4*, 1372.
[177] A. J. Bard, *J. Photochem.* **1979**, *10*, 59.
[178] A. Kudo, *MRS Bull.* **2011**, *36*, 32.
[179] A. Iwase, Y. H. Ng, Y. Ishiguro, A. Kudo, R. Amal, *J. Am. Chem. Soc.* **2011**, *133*, 11054.
[180] Y. Miseki, S. Fujiyoshi, T. Gunji, K. Sayama, *Catal. Sci. Technol.* **2013**, *3*, 1750.
[181] K. Maeda, *ACS Catal.* **2013**, *3*, 1486.
[182] K. Maeda, D. L. Lu, K. Domen, *ACS Catal.* **2013**, *3*, 1026.
[183] S. S. K. Ma, K. Maeda, T. Hisatomi, M. Tabata, A. Kudo, K. Domen, *Chem. Eur. J.* **2013**, *19*, 7480.

[184] H. Kato, Y. Sasaki, N. Shirakura, A. Kudo, *J. Mater. Chem. A* **2013**, *1*, 12327.
[185] K. Sekizawa, K. Maeda, K. Domen, K. Koike, O. Ishitani, *J. Am. Chem. Soc.* **2013**, *135*, 4596.
[186] S. Sato, T. Arai, T. Morikawa, K. Uemura, T. M. Suzuki, H. Tanaka, T. Kajino, *J. Am. Chem. Soc.* **2011**, *133*, 15240.
[187] J. G. Yu, S. H. Wang, J. X. Low, W. Xiao, *Phys. Chem. Chem. Phys.* **2013**, *15*, 16883.
[188] S. F. Chen, L. Ji, W. M. Tang, X. L. Fu, *Dalton. Trans.* **2013**, *42*, 10759.
[189] K. Sayama, K. Mukasa, R. Abe, Y. Abe, H. Arakawa, *J. Photoch. Photobio. A* **2002**, *148*, 71.
[190] K. Maeda, D. Lu, K. Domen, *ACS Catal.* **2013**, *3*, 1026.
[191] H. Kato, M. Hori, R. Konta, Y. Shimodaira, A. Kudo, *Chem. Lett.* **2004**, *33*, 1348.
[192] D. J. Martin, P. J. Reardon, S. J. Moniz, J. Tang, *J. Am. Chem. Soc.* **2014**, *136*, 12568.
[193] X. Wang, S. Li, Y. Ma, H. Yu, J. Yu, *J. Phys. Chem. C* **2011**, *115*, 14648.
[194] H. J. Yun, H. Lee, N. D. Kim, D. M. Lee, S. Yu, J. Yi, *ACS Nano* **2011**, *5*, 4084.
[195] K. P. Xie, Q. Wu, Y. Y. Wang, W. X. Guo, M. Y. Wang, L. Sun, C. J. Lin, *Electrochem. Commun.* **2011**, *13*, 1469.
[196] H. Tada, T. Mitsui, T. Kiyonaga, T. Akita, K. Tanaka, *Nat. Mater.* **2006**, *5*, 782.
[197] H. G. Kim, E. D. Jeong, P. H. Borse, S. Jeon, K. J. Yong, J. S. Lee, W. Li, S. H. Oh, *Appl. Phys. Lett.* **2006**, *89*, 064103.
[198] L. S. Zhang, K. H. Wong, H. Y. Yip, C. Hu, J. C. Yu, C. Y. Chan, P. K. Wong, *Environ. Sci. Technol.* **2010**, *44*, 1392.
[199] P. Zhou, J. Yu, M. Jaroniec, *Adv. Mater.* **2014**, *26*, 4920.
[200] Z. B. Yu, Y. P. Xie, G. Liu, G. Q. Lu, X. L. Ma, H. M. Cheng, *J. Mater. Chem. A* **2013**, *1*, 2773.
[201] A. Iwase, Y. H. Ng, Y. Ishiguro, A. Kudo, R. Amal, *J. Am. Chem. Soc.* **2011**, *133*, 11054.
[202] X. W. Wang, G. Liu, Z. G. Chen, F. Li, L. Z. Wang, G. Q. Lu, H. M. Cheng, *Chem. Commun.* **2009**, 3452.
[203] S. Y. Qin, F. Xin, Y. D. Liu, X. H. Yin, W. Ma, *J. Colloid. Interf. Sci.* **2011**, *356*, 257.
[204] M. Miyauchi, Y. Nukui, D. Atarashi, E. Sakai, *ACS Appl. Mater. Interfaces* **2013**, *5*, 9770.
[205] X. Zong, H. J. Yan, G. P. Wu, G. J. Ma, F. Y. Wen, L. Wang, C. Li, *J. Am. Chem. Soc.* **2008**, *130*, 7176.